Study on the mechanisms governing green leaf volatile-burst caused by tissue-disruption in *Arabidopsis thaliana*

シロイヌナズナにおける傷害応答性みどりの香りバースト機構に関する研究

Satoshi Mochizuki

Graduate School of Sciences and Technology for Innovation

YAMAGUCHI UNIVERSITY

2019

Study on the mechanisms governing green leaf volatile-burst caused by tissue-disruption in *Arabidopsis thaliana*

Satoshi Mochizuki

Graduate School of Sciences and Technology for Innovation

YAMAGUCHI UNIVERSITY

2019

CONTENTS

ABSTRACT

Oxylipins, such as green leaf volatiles (GLVs) and jasmonic acid (JA), were lipid-derived secondary metabolites that are synthesized through the lipoxygenase (LOX) pathway. Oxylipins play a defensive role against herbivore damage, pathogen infection, and so on. LOXs are key enzymes that catalyze an oxygenation of linolenic acid or acyl groups of monogalactosyldiacylglycerol (MGDG), abundant in thylakoid membrane, to form their hydroperoxides. Subsequent cleavage by hydroperoxide lyase (HPL) yields GLVs, or epoxidation/cycliznation by allene oxide synthase (AOS)/allene oxide cyclase (AOC) forms 12-oxo-phytodienoic acid (OPDA) as a precursor of JA. Biosynthetic pathway and physiological function of oxylipins have been extensively studied so far, but the mechanisms to regulate their formation are largely unknown. For example, substantial amount of Arabidopsis LOX2 localizes in chloroplast stroma in intact cell concomitantly with its substrates in thylakoid membrane. Since HPL and AOS localize on chloroplast envelope, plant should have a potential to form GLVs and OPDA continuously. However, plants hardly form oxylipins before suffering stresses. Cell/tissue disruption intimately associated with herbivore damage causes rapid formation of oxylipins (termed as "burst") in nature. Oxylipin-burst is evident within a few seconds–minutes after damage. Subcellular compartment is largely disrupted at the place of damage, and there should be no time to initiate expression of the genes for oxylipin formation. Accordingly, it is suggested that LOX undergoes a system to regulate its enzyme activity at the protein level. In this study, I posed a hypothesis that plant LOXs stays at their inactivated forms in intact tissue to suppress formation of oxylipins and are activated after damage to promptly initiate oxylipin-burst.

In Chapter 1, I identified a specific LOX isoform involved in GLV-burst of Arabidopsis leaves. Plants generally have several LOX isozymes and each of them seems to have specific roles, e.g. GLVs formation, JA formation. So far, a LOX involved in GLVs and/or JA formation has been identified in tobacco, tomato, potato and maize. In Arabidopsis, it is already reported that LOX2 is involved in local formation of JA after tissue disruption. However, the LOX involved in GLVs formation has not been studied largely because the ecotype, Col-0, widely used by plant biologists has a natural mutation in *HPL*. I prepared a complete set of knockout mutant of each *LOX* gene in Ws-1, which has intact *HPL* gene and therefore can form GLVs. Volatiles formed after freeze-thaw treatment of leaves was analyzed with GC-MS. Accordingly, I identified LOX2 as an essential LOX to form GLVs and five carbon volatiles in Arabidopsis.

In Chapter 2, I studied the mechanism to control LOX2 activity. At first, I prepared a recombinant protein with *E. coli* expression system. I found that the activity of recombinant LOX2 is quite unstable that hindered further characterization. Next, I evaluated *ex vivo* LOX2 activity. LC-MS/MS analysis of the extract prepared from disrupted leaves of Col-0 revealed formation of MGDG-hydroperoxides (MGDG-OOHs) as products of LOX2. With considering an analogy with the mechanism to regulate LOX activity in animal tissues, Ca^{2+} was a candidate that regulates activity of Arabidopsis LOX2. Addition of a Ca^{2+} chelating reagent, BAPTA, suppressed formation

of MGDG-OOHs. Formation of GLVs in Ws-1 was also suppressed in the presence of BAPTA, and the amount of GLVs suppressed was mostly same with amount of MGDG-OOHs found in Col-0, which indicated that MGDG-OOHs were largely converted into GLVs. This is the first report that MGDG-OOHs formed by LOX2 is directly involved in GLV-burst in Arabidopsis. GLVs formation was recovered with supplementation of free Ca^{2+} in a dose dependent manner in the presence of BAPTA. BAPTA showed little effect on HPL activity. These results suggest that LOX2 is activated by Ca^{2+} to facilitate GLV-burst in Arabidopsis. A modeling study on Arabidopsis LOX2 based on the structure of coral LOX that is regulated by Ca^{2+} led identification of amino acid residues, which may bind Ca^{2+}, in Arabidopsis LOX2. I examined the effect of Ca^{2+} on the other plant species, such as tobacco, tomato, clover, soybean, rice and maize. Unexpectedly, addition of BAPTA hardly suppressed GLV-burst with these plants.

CHAPTER ONE

Identification of a lipoxygenase involved in biosynthesis of green leaf volatiles in *Arabidopsis thaliana*

Introduction

Oxylipins are metabolites formed from lipids through at least one step of oxygenation reaction catalyzed by lipoxygenases, cyclooxygenases, or α-dioxygenases, and exert a wide variety of bioactivities in plant and animal tissues [1,2]. Green leaf volatiles (GLVs) and jasmonates (JAs) are oxylipins most widely distributed among the plant kingdom. In most cases, the amount of GLVs and JAs are kept low in intact and healthy plant tissues, but their formation is activated upon biotic and abiotic stress stimulus, such as herbivore feeding, pathogen attack, and mechanical wounding [3–5]. GLVs are six carbon aliphatic aldehydes, alcohols, and esters, and have the direct defense effect against microbial pathogens that attempt to invade through wounds on plant tissues as well as the indirect defense function through recruiting predators of herbivores infesting on the plants [3,4] (Fig. 1A). JAs are phytohormones harboring the cyclopenta(e)none moiety in their structures, and involved in stress responses through inducing expression of defense genes and subsequent accumulation of defense metabolites. JAs are also involved in development of plant organs, such as tendril coiling and anther dehiscence [5].

Because GLVs and JAs take distinct functions, the biosynthetic pathways for GLVs and JAs are thought to be under a distinct control. However, most oxylipin biosynthetic pathways share the initial reaction step, i.e., the oxygenation of fatty acids or acyl groups in lipids by a lipoxygenase (LOX) to form their corresponding hydroperoxides. For example, linolenic acid is oxygenated by 13-LOX to form linolenic acid 13*S*-hydroperoxide (13-HPOT). When 13-HPOT would be cleaved by 13-hydroperoxide lyase (13-HPL), (*Z*)-3-hexenal (**2**) would be formed with 12-oxo-(*Z*)-9-dodecenoic acid. On the other hand, when allene oxide synthase (AOS) would act on 13-HPOT, a precursor of JAs, i.e., allene oxide, would be formed, and subsequently converted into 12-oxophytodienoic acid (OPDA) (Fig. 2). There might be two ways to accomplish distinct regulation of each pathway. One way is the distinct spatiotemporal expression of the enzymes next to LOXs, i.e., HPL and AOS [6]. The other way is preparing a distinct set of LOX-HPL and LOX-AOS. It has been reported that tobacco *NaLOX2*, tomato *TomloxC*, potato *StLOX2* (*LOX-H1*), and maize *ZmLOX10* specialize in the GLV pathway [7–10], while rice *OsHI-LOX*, tobacco *NaLOX3*, tomato *TomloxD* and maize *ZmLOX8* specialize in JA pathway [10–13]. It is also reported that one LOX species accounts to both the pathways. For example, rice *OsLOX1* (*OsLOX-L1*) is involved in both the GLV and JA pathways [14]. *TomloxC* mutant also fails to induce JA accumulation after infection of *X. campestris* [8]. Arabidopsis has six LOXs (LOX1 to 6) and four of them (LOX2, LOX3, LOX4, and LOX6) are 13-LOXs that can provide the 13-hydroperoxides for GLV- and JA-biosynthesis, and all the four LOXs are reported to contribute to JA synthesis *in vivo* but in a distinct event [15]. LOX2 is involved in formation of a large amount of JA in wounded leaves [16], while LOX3 and LOX4 are required in JA synthesis essential for male fertility [17]. LOX6 produces JA in the vasculature of leaves [18] as well as in roots [19]. On the contrary, LOX involved in GLV synthesis in Arabidopsis has not been identified. The other two LOXs (LOX1 and LOX5) are 9-LOXs that can provide the 9-hydroperoxides. Oxylipins derived from 9-LOX are reported to regulate lateral root development

and defense responses through a specific signaling cascade, i.e., hypersensitive response, systemic acquired resistance [20,21].

The temporal profiles of formation of GLVs and JAs are also distinctive. GLV formation is rapidly accelerated after disrupting plant tissues [22–24]. In Arabidopsis leaves, induction of **2** formation and emission was evident within a few seconds after mechanical wounding. Such an event, rapid formation and emission after wounding, was termed the 'GLV-burst'. After reaching the maximal levels at 30 to 45 seconds after wounding, the amount of **2** decreased rapidly to the original level [22]. JA formation is also accelerated rapidly after mechanical wounding on Arabidopsis leaves, and the accumulation of JAs was evident at 30 sec after wounding; however, the accumulation of JAs continues until 90 min after wounding [25]. AtLOX6 largely accounts to JA accumulation after mechanical wounding at early timing (<60 sec) [15], and AtLOX2 accounts to it after 90 sec to 90 min [25]. Even though it is evident that disruption of cells caused by mechanical wounding is a trigger to induce rapid formation of GLVs and JAs, we still do not know how the quick oxylipin formation is regulated. In order to get insight into the mechanism supporting the GLV-burst, it is important to identify the step that is activated after wounding.

Isothiocyanates are formed rapidly after tissue disruption. In this case, the precursor (glucosinolates) and the enzyme (myrosinase) that hydrolyzes S-glycoside bonding are compartmentalized from each other at the cellular level. Tissue disruption resulted in mixing the precursor and enzyme to form hydrolyzed products [26]. It has been suggested that a lipase is involved in GLVs pathway to form free linolenic acid from membrane lipids. Therefore, it was often proposed that GLV-burst was supported by activation of the lipid hydrolysis after tissue disruption; however, the lipase(s) involved in GLVs formation has not been identified so far. On the other hand, we previously found that at least part of GLVs was formed without liberation of free fatty acids [27]. In the novel pathway, galactolipids, most abundant lipids in chloroplast membrane, are oxygenated directly by LOX to form galactolipid hydroperoxides. Galactolipid hydroperoxides are subsequently cleaved by HPL to form GLVs and esterified 12 carbon counterparts (Fig. 2) [27]. In this case, LOX and/or its reaction should take a key role in controlling GLV-burst after tissue disruption.

LOX involved in GLV formation in Arabidopsis has not been identified largely because the ecotype Col-0 widely used by plant biologists has a natural mutation of HPL, and hardly forms GLVs [28]. In this study, I prepared a complete set of mutants deficient in each LOX gene in Arabidopsis with Ws-1 or L*er* background to identify the LOX essential to formation of GLVs. Detailed analysis of GLVs and related compounds with each mutant line prompted us to assume the mechanism supporting the GLV-burst.

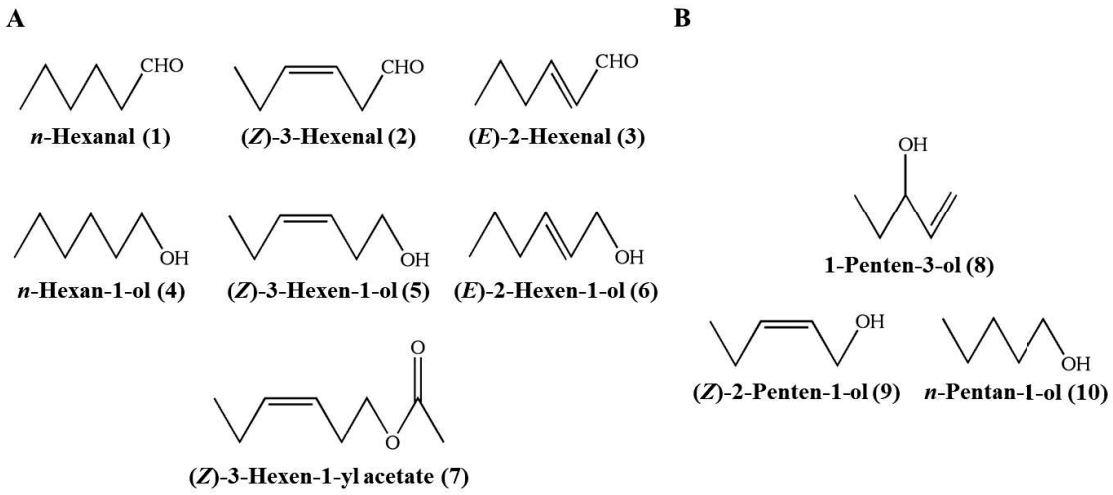

Fig. 1. Chemical structures of volatile compounds mentioned in this Chapter. A, GLVs. B, Five carbon (C5) volatiles.

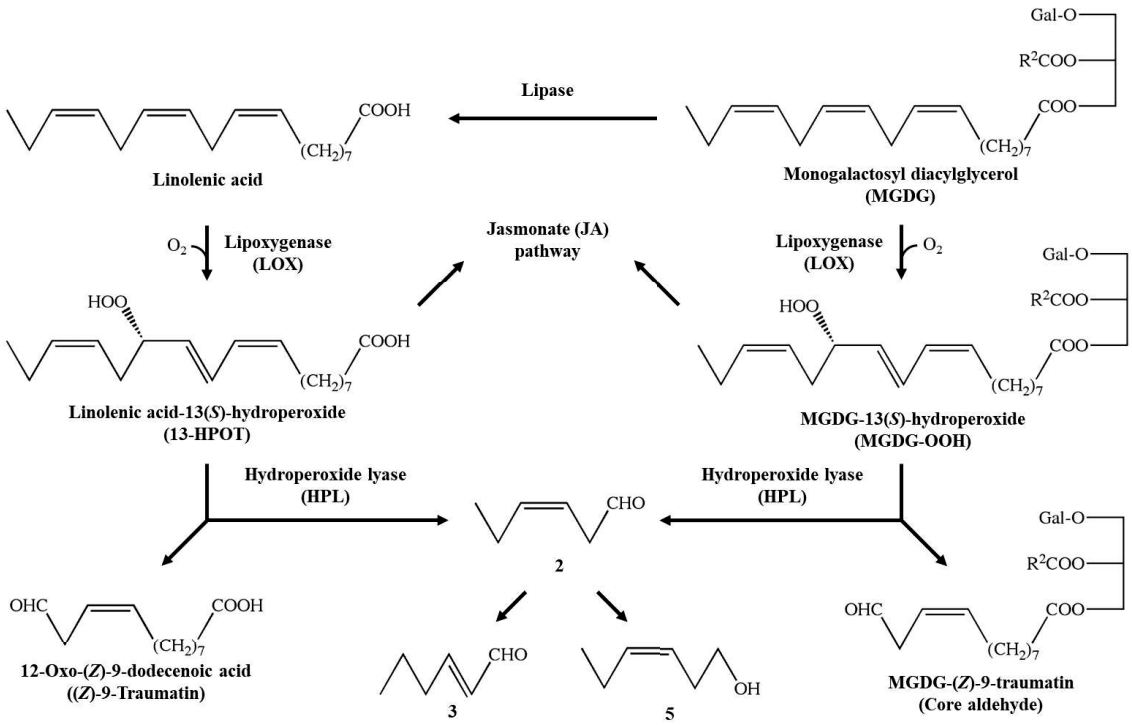

Fig. 2. The biosynthetic pathway of GLVs in Arabidopsis.

Materials and Methods

Plant materials

Arabidopsis thaliana mutants *lox1* (FLAG_156H09), *lox3* (FLAG_071B05), *lox4* (CSHL_GT7719), *lox5* (FLAG_579D04), *lox6* (SALK_047440) were obtained from Versailles Arabidopsis Stock Center (http://publiclines.versailles.inra.fr/) [29]. *lox1*, *3*, *5* are in Ws-1 background, and *lox4* is L*er* background. *lox2-1* and *lox6* mutant in Col-0 background were crossed with Ws-1 and homozygous mutant in Ws-1 backgrounds were generated. Original *lox2-1* mutant (Col-0) was given from Dr. Edward E. Farmer (Université de Lausanne, Switzerland). For experiments presented in Figs. 1–8, and 16A, *Arabidopsis thaliana* wild-type (Col-0, Ws-1, and L*er*) and *lox* mutants were grown at 25°C with 50% humidity, under 14 h of light/day (fluorescent lights at 50–150 μmol m^{-2} s^{-1}) for 23–36 days. For other experiments, plants were grown at 22°C, 50–150 μmol m^{-2} s^{-1}, under 10 h of light/day (fluorescent lights at 50–150 μmol m^{-2} s^{-1}) for 42–49 days.

Genotyping PCR and semi-quantitative RT-PCR

Genotyping PCR was carried out with genomic DNA extracted from Arabidopsis leaves (Fig. 3A). Arabidopsis leaves (100 mg) were homogenized with 665 μL of extraction buffer (0.1 M Tris-HCl pH 8.0, 0.7 M NaCl, 50 mM EDTA). After incubation at 65°C for 15 min, 325 μL of chloroform: isoamyl alcohol solution (24:1, v/v) was added, and then, incubated for 5 min. After centrifugation at 14,000 rpm for 2 min at 25°C, supernatant (about 400 μL) was mixed with 700 μL of isopropanol, then, centrifuged at 14,000 rpm for 10 min at 25°C. The precipitate was suspended with distilled H_2O and used as genomic DNA [30]. KOD FX Neo (TOYOBO, Osaka, Japan) was used for PCR. For genotyping of *lox2-1* mutant, I followed protocol described by Glauser (2009) [25]. Agarose gel (*AtLOX1–6*) and polyacrylamide gel (*AtHPL*) electrophoresis were used.

Semi-quantitative RT-PCR was carried out with first strand cDNA prepared from total RNA extracted from Arabidopsis leaves (Fig. 3B). Total RNA was extracted with RNeasy mini kit (QIAGEN) and DNase I (TAKARA BIO), and cDNA was obtained from total RNA with SuperScript III (Thermo Fisher Scientific). KOD FX Neo was used for PCR. Primer list is shown in Table. 1.

Freeze-thaw and time course assay with GC-MS

Above-ground part of Arabidopsis were cut out with razor blade and immediately snap-frozen with liquid nitrogen. In order to determine the GLVs levels in intact tissues, cold solvent (at −80°C) was directly mixed with the frozen plant tissue powder in a closed vial. For freeze-thaw or time course assay, frozen plant tissue powder was thawed at 25°C in a closed vial, and incubated further for a given time before extraction with the solvent. The enzyme reaction was terminated by adding 2 mL of methyl *tert*-butyl ether (MTBE) containing 10 ng μL^{-1} of *n*-nonan-1-yl acetate (Tokyo Chemical Industry Co., Tokyo, Japan) as an internal standard (IS). After incubation for 10 min at 60°C, the MTBE mixture was centrifuged at 1,500 rpm for 10 min at 25°C. A portion (1 μL) of the extract was subjected to GC-MS (QP-5050, Shimadzu, Kyoto, Japan) equipped with a DB-WAX column (30 m length × 0.25 mm diameter × 0.25 μm film thickness, Agilent Technologies). Injection was carried out using a splitless mode with a splitless sleeve (Shimadzu, Kyoto, Japan). The sampling time was 1 min, and vaporization chamber temperature was 240°C. The initial oven temperature was 40°C, held for 5 min, ramped at 3.5°C min^{-1} to 100°C. The carrier gas (He) was delivered at 44.8 cm s^{-1}. The MS was operated in the electron ionization mode with ionization energy of 70 eV, and the temperatures of the ion source and interface were 200°C and 240°C, respectively, with a continuous scan from *m*/*z* 40 to 350. In order to identify each compounds, retention indices and MS profiles of corresponding authentic specimens were used. In order to construct calibration curves for quantification, *n*-hexanal (**1**) (Wako Pure Chemicals, Osaka, Japan), **2** (Nihon Zeon, Tokyo, Japan), (*E*)-2-hexenal (**3**) (Wako Pure Chemicals, Osaka, Japan), (*Z*)-3-hexen-1-ol (**5**) (Wako Pure Chemicals, Osaka, Japan), 1-penten-3-ol (**8**) (Alfa Aesar, Ward Hill, MA), (*Z*)-2-penten-1-ol (**9**) (Alfa Aesar, Ward Hill, MA), and *n*-pentan-1-ol (**10**) (Sigma-Aldrich, St. Louis, MO) were dissolved in MTBE containing *n*-nonan-1-yl acetate, and then subjected to GC-MS (Fig. 8). Unfortunately, there was a contamination of *o*-xylene at the same retention time with that of **2** (Fig. 5A). In order to quantify the amount of **2** precisely, selected-ion monitoring chromatogram (SIM) with representative fragment ion, which is 69 *m/z* (Da) (Fig. 5B), was used to construct the calibration curve to quantify.

HPL activity analysis by using HPLC

The above-ground part (1 g FW) of Arabidopsis plant were homogenized with homogenization buffer (2 mL of 50 mM Na phosphate pH 6.3 containing 50 mM diethylenetriaminepentaacetic acid) with a mortar and pestle to give crude enzyme solution. The crude enzyme (100 μL) was mixed with 10 μL of 0.1 mM of 13-HPOT prepared from α-linolenic acids (Sigma-Aldrich) with soybean lipoxygenase in ethanol in 1 mL of reaction mixture (Figs. 10, 11, 12A, and 12B) [31]. In some experiments (Fig. 12C), 13-HPOT and *O*-(13*S*-hydroperoxy-(9*Z*,11*E*,15*Z*)-9,11,15-octadecatrienoyl)-*O*-(11*S*-hydroperoxy-(7*Z*,9*E*,13*Z*)-7,9,13-hexadecatrienoyl) monogalactosyl diglyceride (MGDG-13-HPOT/11-HPHT) in ethanol were used as a substrate. MGDG-13-HPOT/11-HPHT was obtained from conversion of *O*-(9*Z*,12*Z*,15*Z*)-9,11,15-octadecatrienoyl-*O*-(7*Z*,10*Z*,13*Z*)-7,9,13-hexadecatrienoyl) monogalactosyl diglyceride (MGDG-C18:3/C16:3) to hydroperoxides by using soybean lipoxygenase. MGDG-C18:3/C16:3 was purified from spinach leaves [27]. MGDG-13-HPOT/11-HPHT and 13-HPOT (14.04 μL of 1.78 mM and 15 μL of 3.3 mM, respectively) were used to give same amount of corresponding hydroperoxides for HPL. After 3 min incubation at 25°C, 1 mL of 0.1% (w/v) 2,4-dinitrophenylhydrazine in ethanol containing 0.5 M acetic acid and 50 μL of 0.1 mM *n*-heptanal (Wako Pure Chemicals, Osaka, Japan) as an internal standard were mixed. After incubation for 1 h in the dark, the hydrazone derivatives were extracted with 2 mL of *n*-hexane. After drying up the *n*-hexane extract, the residue was dissolved in 200 μL of acetonitrile. Compound **2** formed during the reaction was quantified with HPLC (Prominence, Shimadzu) equipped with a Mightysil RP-18GP (2.0 × 150, 5 μm) column with the isocratic solvent system, acetonitrile: water: formic acid (65:35:0.1, v/v/v) at the flow rate of 0.2 mL min^{-1} at 40°C with following absorbance with a photodiode array detector (SPD-M10A, Shimadzu). In order to identify **2**, the retention time and the spectrum of corresponding authentic standard were used. The calibration curve was constructed with authentic **2** suspended in 1 mL of the homogenate buffer (Fig. 12). In order to evaluate HPL activity in each crude enzyme (Fig. 11A), the amount of **2** formed in the presence of substrate was subtracted from that formed in the absent of substrate.

SPME analysis

After cutting the hypocotyl close to the hypocotyl-root junction, the above-ground parts of Arabidopsis plants were placed on the cap of vial (Micro tube 2 mL, 72.693, SARSTEDT, Tokyo, Japan) with a portion of tap water, and then placed into a glass jar (187 mL, 67 mm diameter, 75 mm height) (Fig. 13D). In wounding treatment, about 20% area of apical part of all odd number leaves were wounded by pinching with forceps The leaves were numbered from youngest to oldest (Figs. 13A, 13B, and 13C). A SPME fiber (50/30 μm DVB/Carboxen/PDMS, Supelco) was exposed to the headspace immediately after placing the plants in the jar, then, the volatiles were collected for 30 min at 25°C (Fig. 13D). After collection, the fiber was inserted into the insertion port of a GC-MS. GC-MS analysis of the volatiles were carried out with direct insertion of the fiber into the injection port of GC-MS equipped with SPME Sleeve (Shimadzu, Kyoto, Japan). The conditions were as shown above but rate of temperature increase from 40 to 95°C was reduced to 3.25°C min^{-1} to get better separation. The fiber was held in the injection port (set at 240°C) for 10 min to fully remove any compounds from the matrix. In order to identify each compounds, MS profiles of corresponding authentic specimens were used. In order to construct calibration curves for quantification, **2** (Nihon Zeon, Tokyo, Japan), **3** (Wako Pure Chemicals, Osaka, Japan), **5** (Wako Pure Chemicals, Osaka, Japan), *n*-hexan-1-ol (**4**) (Tokyo Chemical Industry Co., Tokyo, Japan), (*Z*)-3-hexen-1-yl acetate (**7**) (Wako Pure Chemicals, Osaka, Japan), (*E*)-2-hexen-1-ol (**6**) (Wako Pure Chemicals, Osaka, Japan), **8** (Alfa Aesar, Ward Hill, MA), and **9** (Alfa Aesar, Ward Hill, MA) were suspended in 3.5% (w/v) Tween 20. Two sheets of filter paper (grade 391, 55 mm diameter, MUNKTELL) infiltrated with 150 μL of the volatile-suspension were placed inside of the jar to give almost similar surface area with plant leaves (Fig. 16). The quantification of **2** was done with representative fragment ion of $m/z = 69$ (as described above).

Phylogenetic analysis

Phylogenetic analyses were carried out using the Maximum Likelihood method and the Neighbor-joining method based on the LG model + G + I (8 categories) in MEGA6 (Fig. 19). Amino acid sequences were aligned using MAFFT v7.220 [31]. Genbank accession numbers of each LOX proteins used for phylogenetic analysis were described in Table. 2.

Statistics

All values are presented as means ± SEM. Statistical analyses were performed with BellCurve in Microsoft Excel (Social Survey Research Information Co., Tokyo, Japan). Statistical methods used are described in the captions of figures.

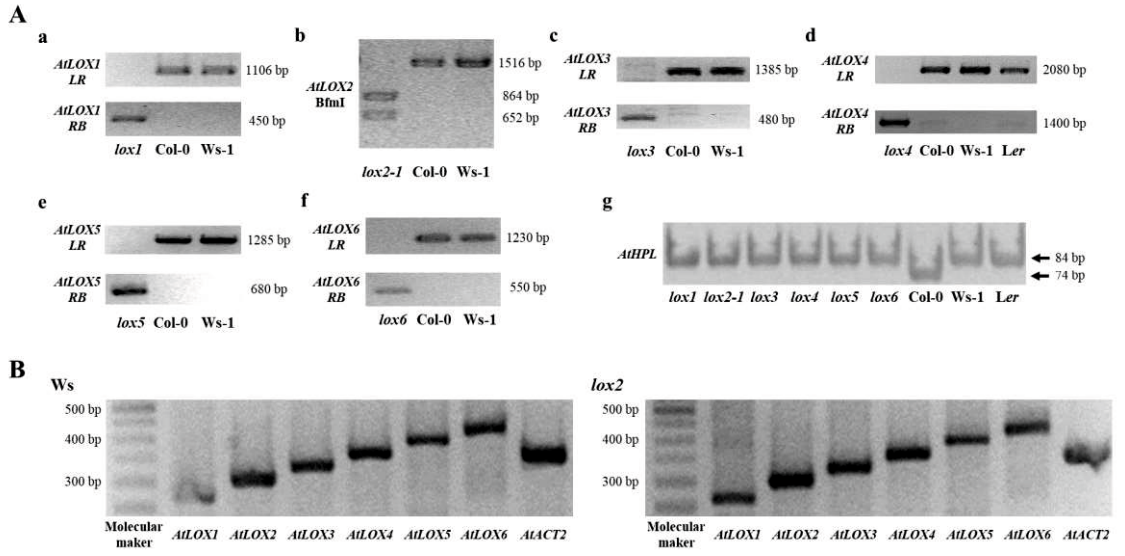

Fig. 3. Genotyping and semi-quantitative RT-PCR. A, Genotyping of *AtLOXs* in each mutant lines. Each *lox* mutants except *lox2-1* are T-DNA insertion mutant. B, Expression of *AtLOXs* in leaf in Ws-1 and *lox2-1* mutant. Ws-1 and *lox2-1* mutant have a same expression profile in *AtLOXs*. Primer set for genotyping and semi-quantitative RT-PCR are found in Table. 1.

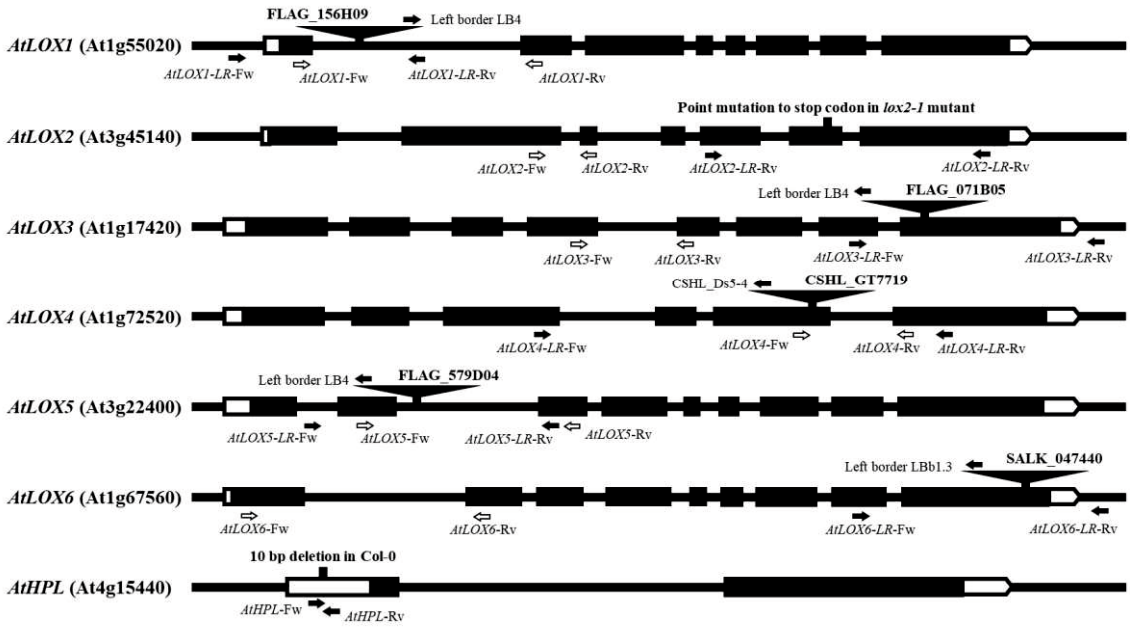

Fig. 4. Schematic map of *AtHPL* and *AtLOXs*. Filled arrows indicate primers used for genotyping, and open arrows indicate primers used for RT-PCR.

A

Target for genomic PCR	Primer set
AtLOX1-LR	*AtLOX1-LR*-Fw and *AtLOX1-LR*-Rv
AtLOX1-BR	*AtLOX1-LR*-Rv and Left border LB4
AtLOX2-LR	*AtLOX2-LR*-Fw and *AtLOX2-LR*-Rv
AtLOX3-LR	*AtLOX3-LR*-Fw and *AtLOX3-LR*-Rv
AtLOX3-BR	*AtLOX3-LR*-Fw and Left border LB4
AtLOX4-LR	*AtLOX4-LR*-Fw and *AtLOX4-LR*-Rv
AtLOX4-BR	*AtLOX4-LR*-Fw and CSHL_Ds5-4
AtLOX5-LR	*AtLOX5-LR*-Fw and *AtLOX5-LR*-Rv
AtLOX5-BR	*AtLOX5-LR*-Fw and Left border LB4
AtLOX6-LR	*AtLOX6-LR*-Fw and *AtLOX6-LR*-Rv
AtLOX6-BR	*AtLOX6-LR*-Rv and Left border LBb1.3
AtHPL	*AtHPL*-Fw and *AtHPL*-Rv

B

Primer for genomic PCR	Sequence
AtLOX1-LR-Fw	TTTGGGATCTTCGTCATACCC
AtLOX1-LR-Rv	AAAACAAATTGAAATAATTAGCACG
AtLOX2-LR-Fw	GGATTATCATGATTTGCTTCTACC
AtLOX2-LR-Rv	TCAAATAGAAATACTATAAGGAACAC
AtLOX3-LR-Fw	ACGTTGGAAATCAATGCTTTG
AtLOX3-LR-Rv	CTCTCAAGTGAATGGCTGAGG
AtLOX4-LR-Fw	GCTGCATGTAGACTTAAGGCG
AtLOX4-LR-Rv	AGAGTACCAGGCTTGGAGCTC
AtLOX5-LR-Fw	CGACCCGTTATCAAATCCATC
AtLOX5-LR-Rv	TGATTAGCTCCGGTGTTTCAC
AtLOX6-LR-Fw	AGTTGAGTACAATGCATCCGG
AtLOX6-LR-Rv	ATAGCCAGTGACTCCATGTGG
AtHPL-Fw	GTTGGACCATTATCGGACCGTTTAG
AtHPL-Rv	CTTATACTTCTCAGCTCTTGTCCGG
Left border LB4	CGTGTGCCAGGTGCCCACGGAATAGT
CSHL_Ds5-4	TACGATAACGGTCGGYACGG
Left border LBb1.3	ATTTTGCCGATTTCGGAAC

C

Target for semi-quantitative RT-PCR	Primer set
AtLOX1	*AtLOX1*-Fw and *AtLOX1*-Rv
AtLOX2	*AtLOX2*-Fw and *AtLOX2*-Rv
AtLOX3	*AtLOX3*-Fw and *AtLOX3*-Rv
AtLOX4	*AtLOX4*-Fw and *AtLOX4*-Rv
AtLOX5	*AtLOX5*-Fw and *AtLOX5*-Rv
AtLOX6	*AtLOX6*-Fw and *AtLOX6*-Rv
AtACT2	*AtACT2*-Fw and *AtACT2*-Rv

D

Primer for semi-quantitative RT-PCR	Sequence
AtLOX1-Fw	GGAAATGAGACGACGACGAAG
AtLOX1-Rv	TCGAACGTGACCTTGAAAGC
AtLOX2-Fw	ACTTCATTCACAGGCAAGGC
AtLOX2-Rv	GATTAAGGCCGGCAAGTGTC
AtLOX3-Fw	TGTAGCTGAGGACTTTGCAGAC
AtLOX3-Rv	TAAGAGCGGAGTGTTGTGGAC
AtLOX4-Fw	CCACCAGCTTGTGAATCATTGG
AtLOX4-Rv	TGGCGTATGGGTAGTCTTCAAC
AtLOX5-Fw	TGAGGAAACTGCGTTTGGAG
AtLOX5-Rv	TGAGTCAGGACCCTTGTCAG
AtLOX6-Fw	ACGAACTTCAACGGCGTCAG
AtLOX6-Rv	TCTTTCACAGCCTTTGGGAGTC
AtACT2-Fw	TGCCCAGAAGTCTTGTTCCAG
AtACT2-Rv	TGTGAACGATTCCTGGACCTG

Table. 1. Primers for genotyping and RT-PCR. A and C, Primer set for genotyping and RT-PCR (Figs. 3A and 3B). B and D, Sequences of primer for genotyping and RT-PCR.

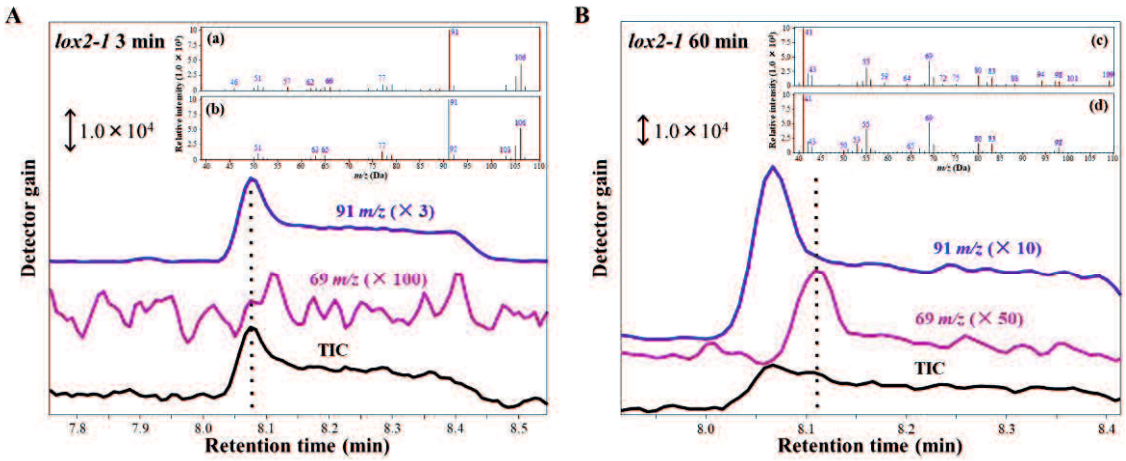

Fig. 5 The quantification of 2 with selected-ion monitoring chromatogram (SIM) by using representative fragmented ions. The peak of retention time of **2** was overlapped with the peak of *o*-xylene. In order to quantify precisely, the representative fragmented ion of **2** (*m/z* of 69) was used. A, The chromatogram of 3 min freeze-thaw treated *lox2-1* (black: Total ion chromatogram (TIC), pink: 100 times expanded *m/z* of 69, blue: 3 times expanded *m/z* of 91 (representative fragmented ion of *o*-xylem). (a) indicates the MS profile of the peak indicated with the dashed line in A. (b) indicates the MS profile of *o*-xylem. B, The chromatogram of 60 min freeze-thaw treated *lox2-1* (black: TIC, pink: 50 times expanded *m/z* of 69, blue: 10 times expanded *m/z* of 91). (c) indicates the MS profile of the peak indicated with the dashed line in B. (d) indicates the MS profile of **2**.

Results

Volatiles formed in Arabidopsis after freeze-thaw treatment

In order to determine the GLV and C5 volatile levels in intact leaf tissues, cold solvent (chilled at –80°C) was directly mixed with the frozen leaf powder prepared from leaves snap-frozen with liquid N_2 with suppressing any enzyme reactions during the extraction process. The other portion of the frozen leaf powder was thawed at 25°C in a closed vial, and incubated further for 3 min to facilitate enzyme reactions before extraction with the solvent. With the wild type ecotypes, Ws-1 and L*er*, low but substantial amounts of GLVs and C5 volatiles were detected even in the intact leaves, and **2** was most abundant among the volatiles quantified here (Figs. 6 and 7). The freeze-thaw treatment followed by 3 min-incubation at 25°C extensively facilitated formation of **2**,**3**, and **5** in both Ws-1 and L*er*, but the amounts of **1**, and C5 volatiles, such as **8**, **9**, or **10**, showed little changes (Fig. 7). Because I used completely disrupted tissues, **7** acetate that could be detected in partially wounded leaves, especially in the headspace (Fig. 15) [23], was hardly detected. In Col-0, the amounts of **2** and **3** were much less than those found in Ws-1 and L*er*, because Col-0 lacked HPL activity [28]. The amount of **1** in intact Col-0 leaves was equivalent to those in intact Ws-1 and L*er*, but the freeze-thaw treatment significantly increased its amount only in Col-0. The levels of C5 volatiles in Col-0 were not different from those in the other two ecotypes, but the amounts **8** slightly increased after freeze-thaw treatment.

The amounts of GLVs and C5 volatiles detected in intact leaves of *lox1* (Ws-1)*, lox3* (Ws-1)*, lox4* (L*er*)*, lox5* (Ws-1)*, and lox6* (Ws-1) mutants were largely similar to the corresponding wild type ecotypes. The effect of freeze-thaw treatment on the amounts of GLVs and C5 volatiles were also similar to the corresponding wild type ecotypes, and those of GLVs increased rapidly but those of C5 volatiles showed little changes. The amounts of GLVs and C5 volatiles detected either in intact or in freeze-thaw treated *lox2-1* (Ws-1) leaves were significantly lower than those in the other Arabidopsis genotypes and ecotypes (Figs. 6 and 7). Compound **10** was an exception, and its amount was largely constant irrespective of the genotypes, ecotypes, and freeze-thaw treatment.

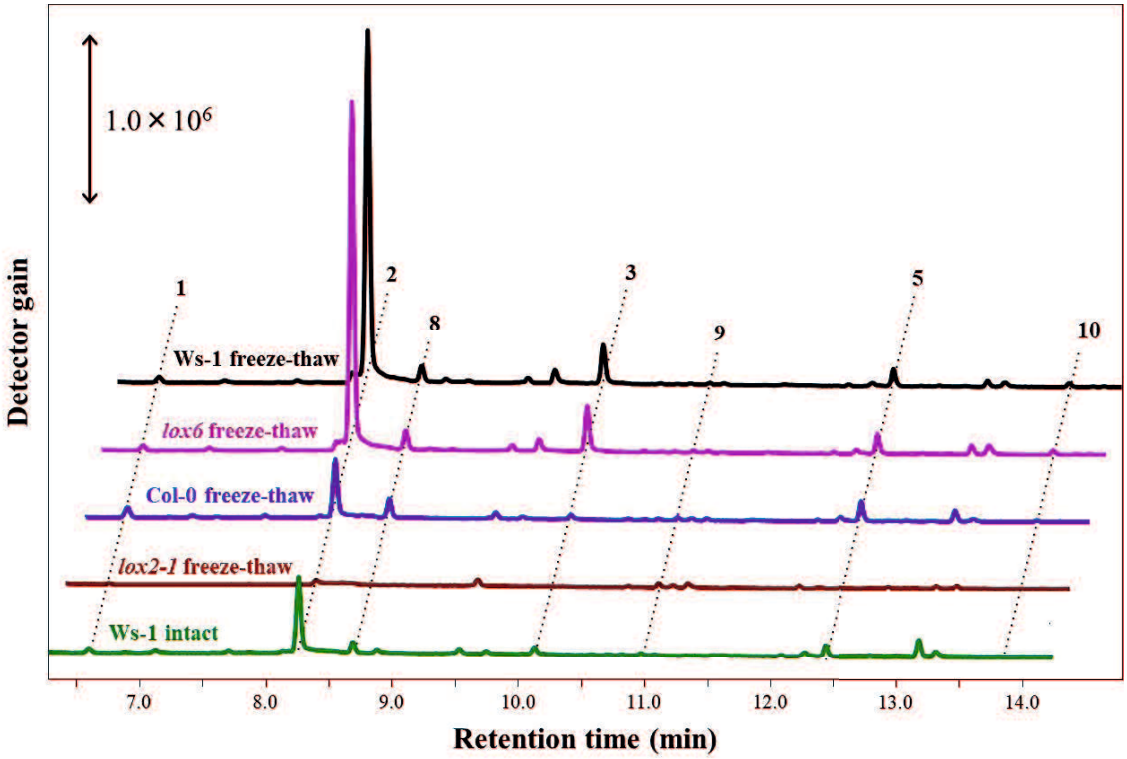

Fig. 6. Effect of freeze-thaw treatment on GLVs and C5 volatiles in Arabidopsis. Arabidopsis tissue powder was freeze-thaw treated and subsequently incubated for 3 min, and volatile compounds were collected by extraction with MTBE. Representative chromatograms were shown (black: freeze-thaw treated Ws-1, pink: freeze-thaw treated *lox6*, blue: freeze-thaw treated Col-0, brown: freeze-thaw treated *lox2-1*, and green: intact Ws-1).

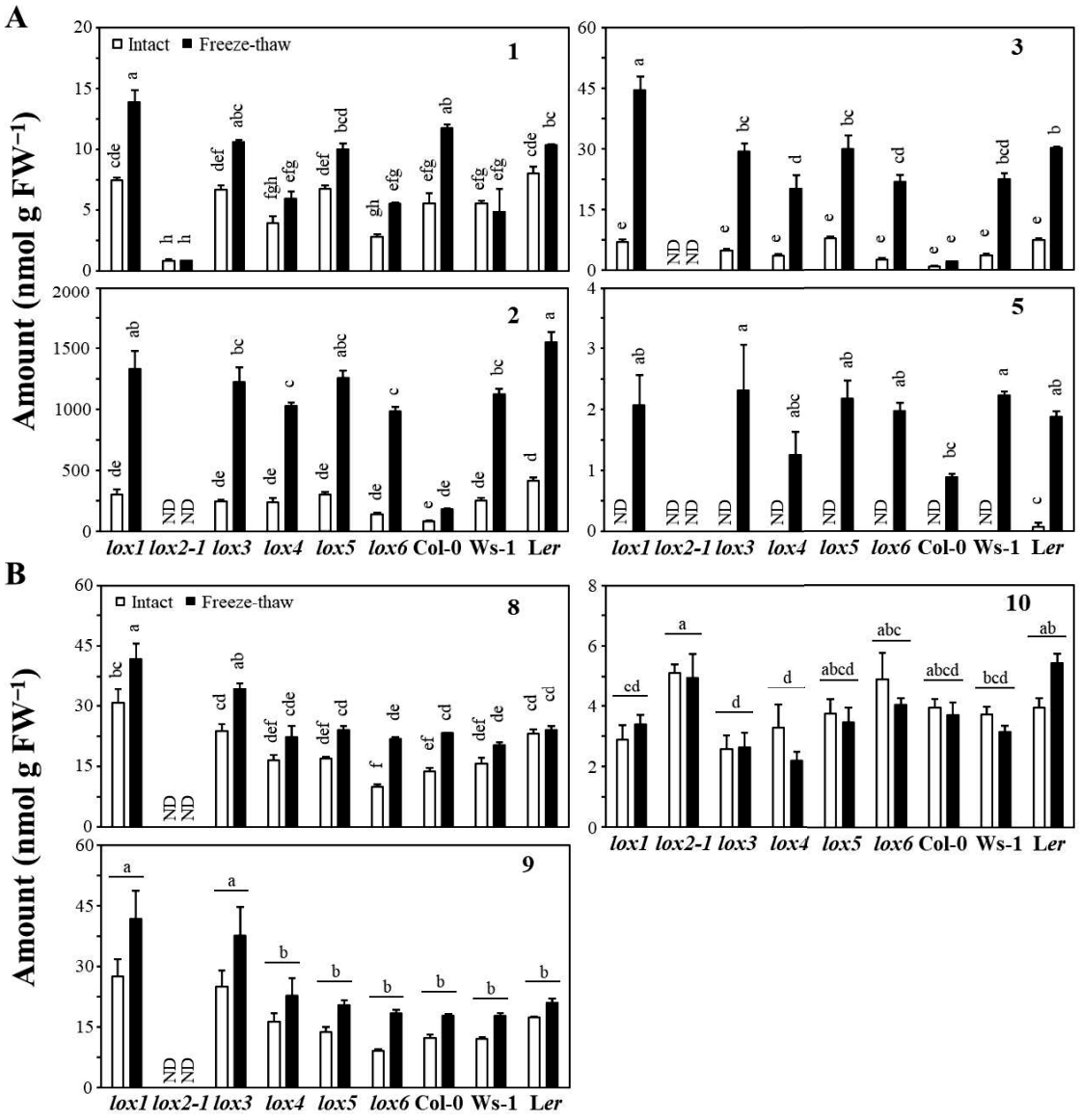

Fig. 7. Formation of GLVs and C5 volatiles in Arabidopsis requires the activity of LOX2. A, The amount of GLVs in intact and freeze-thaw treated Arabidopsis. B, The amount of C5 volatile compounds in intact and freeze-thaw treated Arabidopsis. Mean values ± SEM (error bars) are shown (n = 3, technical replicates). Different letters show significant difference (two-way ANOVA, Tukey, $P < 0.05$). In the amount of **9**, there is significant difference in genotype (among mutants and wild types) and treatment (intact vs freeze-thaw), respectively (two-way ANOVA, Tukey, $P < 0.01$), but there is no significant difference in interaction effect between genotype. In the amount of *n*-pentanl-1-ol, there is significant difference in genotype (two-way ANOVA, Tukey, $P < 0.01$), but no significant difference in treatment. Different letters in **9** and **10** show significant differences among genotype. ND, not detected.

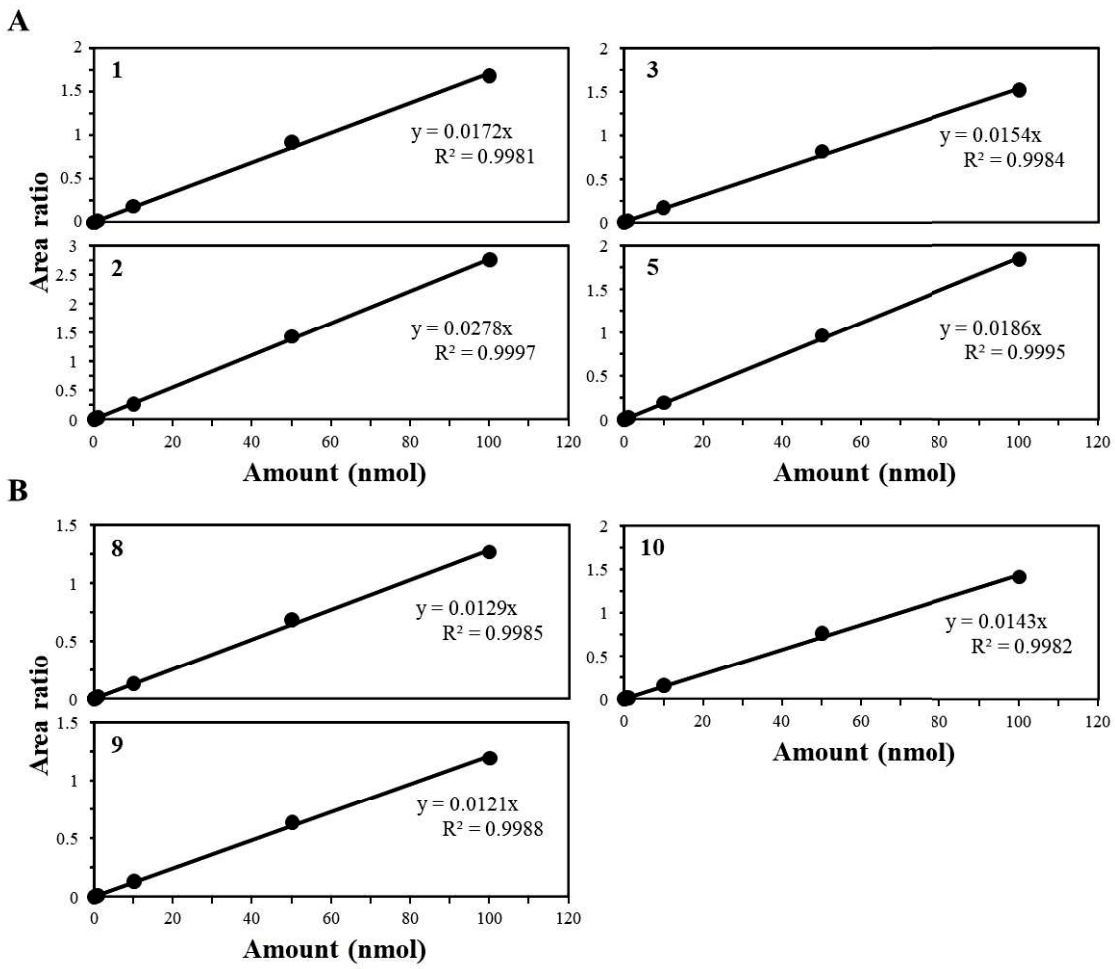

Fig. 8. Calibration curves used for the quantification of GLVs and C5 volatiles. These calibration curves were used to quantify the amount after solvent extraction (Figs. 7 and 17).

HPL activity in *lox2-1* mutant

LOX2 is most accountable to biosynthesis of JA after mechanical wounding of Arabidopsis leaves [16]. HPL is under regulation of JA signaling [6]. Therefore, it was anticipated that low amounts of GLVs in *lox2-1* mutant was caused by low HPL activity in this mutant. In order to determine HPL activity in *lox2-1* mutant, I examined the HPL activity by using HPLC (Figs. 9 and 10). The most abundant product of HPL, **2**, was quantified as a hydrazone derivative after adding substrate (13-HPOT and MGDG-13-HPOT/11-HPHT). I found that the *lox2-1* mutant showed substantial HPL activity even larger than that in Ws-1 wild type ecotype (Fig. 11). Therefore, the low ability to form GLVs in *lox2-1* mutant was not caused by a change in HPL activity but largely caused by impairment of LOX2 activity. There is significant difference between the amounts of **2** formed from 13-HPOT with Ws-1 and *lox2-1*.

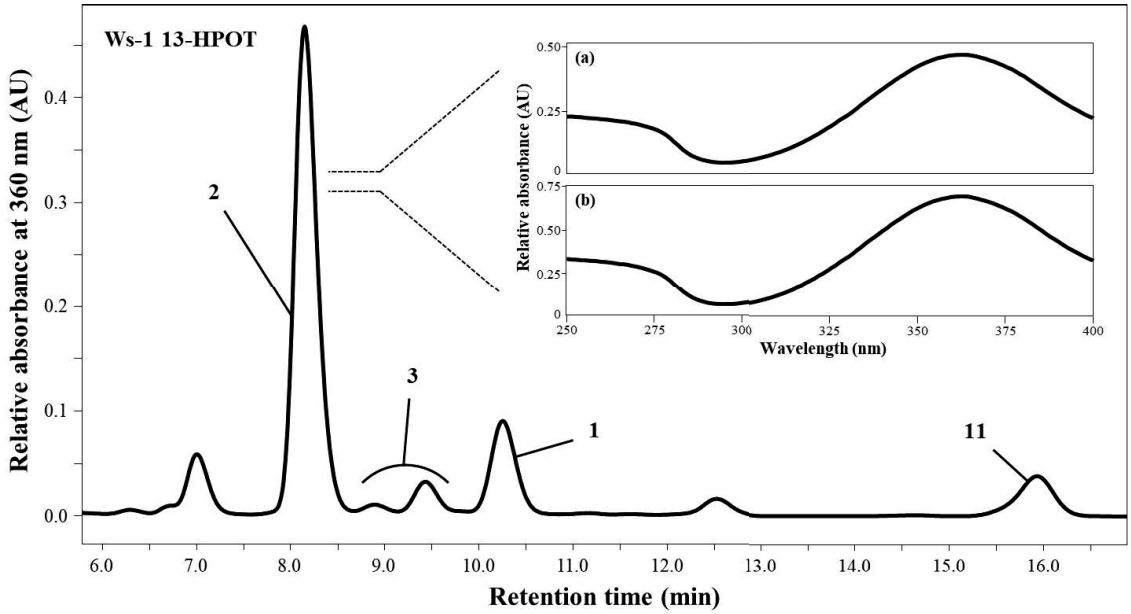

Fig. 9. Detection of GLVs from Arabidopsis upon adding 13-HPOT by using HPLC. After mixing Arabidopsis homogenate with 13-HPOT, the products were converted into hydrazine derivatives, and hydrazone derivatives of GLVs were analyzed by using HPLC with following absorption at 360 nm. Representative chromatogram of Ws-1 with 13-HPOT, and spectrum of **2** at retention time of 8.2 min were shown. (a); the spectrum obtained from Ws-1 with 13-HPOT, (b); the spectrum obtained from authentic standard. 11, *n*-heptanal (IS).

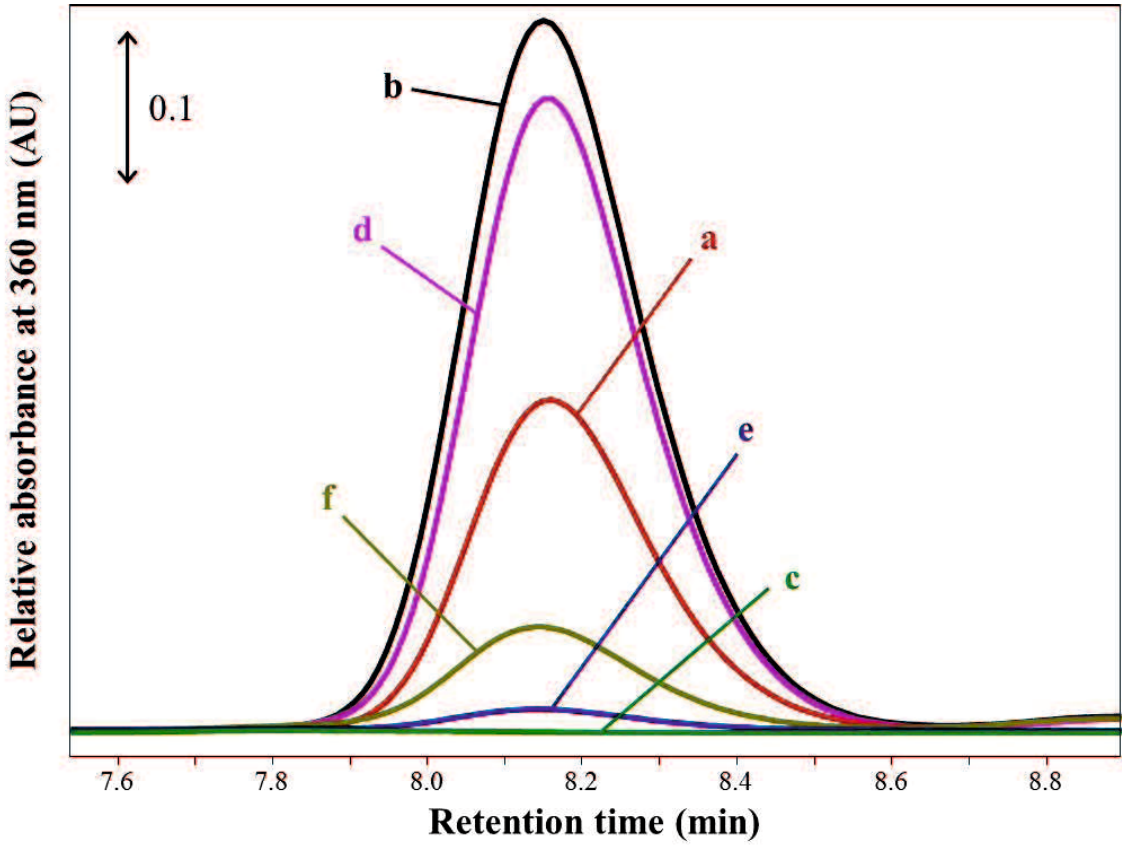

Fig. 10. Representative chromatograms of 2 in Arabidopsis Col-0, Ws-1 and *lox2-1* mutant. a, Ws-1 Control, b, Ws-1 with 13-HPOT, c, *lox2-1* Control, d, *lox2-1* with 13-HPOT, e, Col-0 Control, f, Col-0 with 13-HPOT).

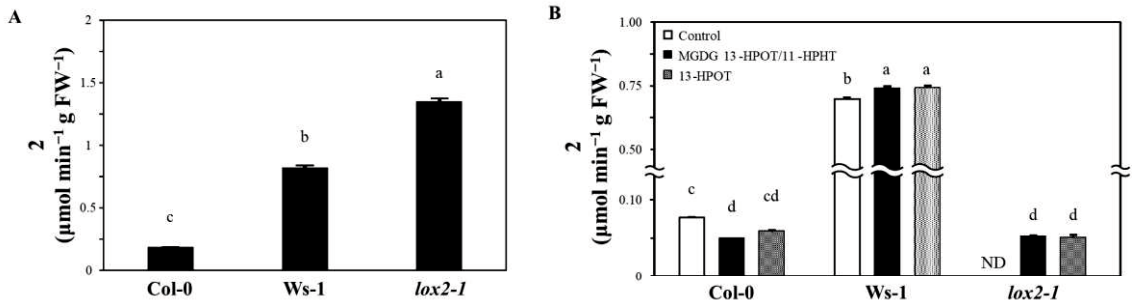

Fig. 11. HPL activity in Arabidopsis *lox2-1* mutant. A, HPL activity in crude extract prepared from Col-0, Ws-1, and *lox2-1* leaves. HPL activity was evaluated as the formation of the amount of **2** in the presence of 13-HPOT. Mean values ± SEM (error bars) are shown (n = 4, technical replicates). Asterisks show significant difference (one-way ANOVA, Tukey, $P < 0.01$). B, The amount of **2** in crude extract from Arabidopsis with MGDG-13-HPOT/11-HPHT and 13-HPOT. Supplementation of 25 nmol of MGDG-13-HPOT/11-HPHT or 50 nmol of 13-HPOT was 25 nmol of MDGD-13-HPOT/11-HPHT or 50 nmol of 13-HPOT was mixed into 1 mL reaction mixture. Mean values ± SEM (error bars) are shown (n = 4, technical replicates). Asterisks show significant difference (two-way ANOVA, Tukey, $P < 0.05$). ND, not detected.

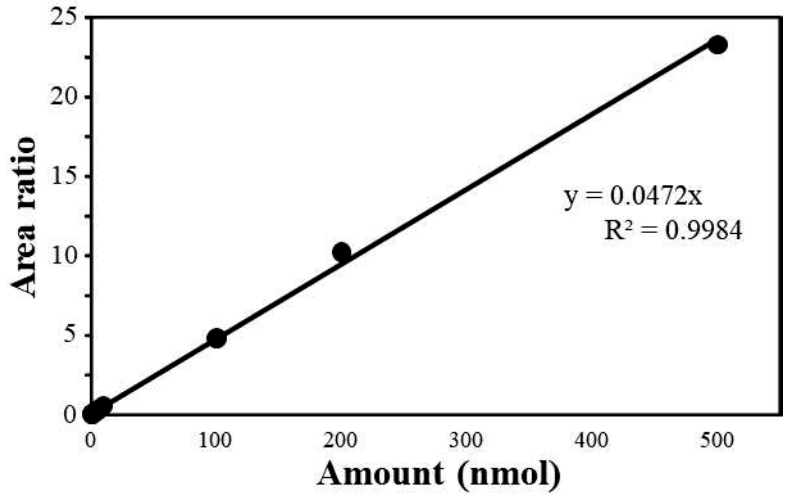

Fig. 12. The calibration curve of 2 used for the quantification. The peak area integrated with following absorption at 360 nm was used for quantification.

Volatiles formed from partially wounded Arabidopsis leaves

I evaluated the requirement of LOX2 in GLVs and C5 volatile formation through analyzing emission of them from partially wounded leaves. Because involvement of LOX6 in JA formation in systemic leaves of wounded plant was indicated [15], *lox6* mutant was also used for the analysis. Apical part (about 20% of total leaf area) of odd numbered leaves were wounded by pinching with forceps, and the volatiles emitted into headspace were collected with a SPME fiber for 30 min (Fig. 13). From intact leaves, the amounts of GLVs and C5 volatiles were under detection limit with exception of **4**. In partially wounded Ws-1 leaves, the amounts of GLVs and C5 volatiles significantly increased (Fig. 14). We previously found that in partially wounded Arabidopsis leaves **2** formed in the disrupted tissues diffused into the neighboring intact tissues where **2** was reduced by a NADPH-dependent reductase to yield **5**, and subsequently acetylated to form **7** [23]. Therefore, from wild type Ws-1 leaves, the amount of **5** was highest among GLVs, followed by **2** and **7** (Fig. 15). **8** and **9** were also detected but **10** was under the detection limit. This was almost the case with *lox6* mutant and the volatile profiles in intact and freeze-thaw disrupted leaves showed no significant difference from those found with Ws-1. Emission of GLVs after partial wounding was hardly observed with Col-0 even though the amount of **4** and C5 volatiles significantly increased to the level found with Ws-1 ecotype. On the other hand, *lox2-1* mutant emitted undetectable GLVs even after partial wounding.

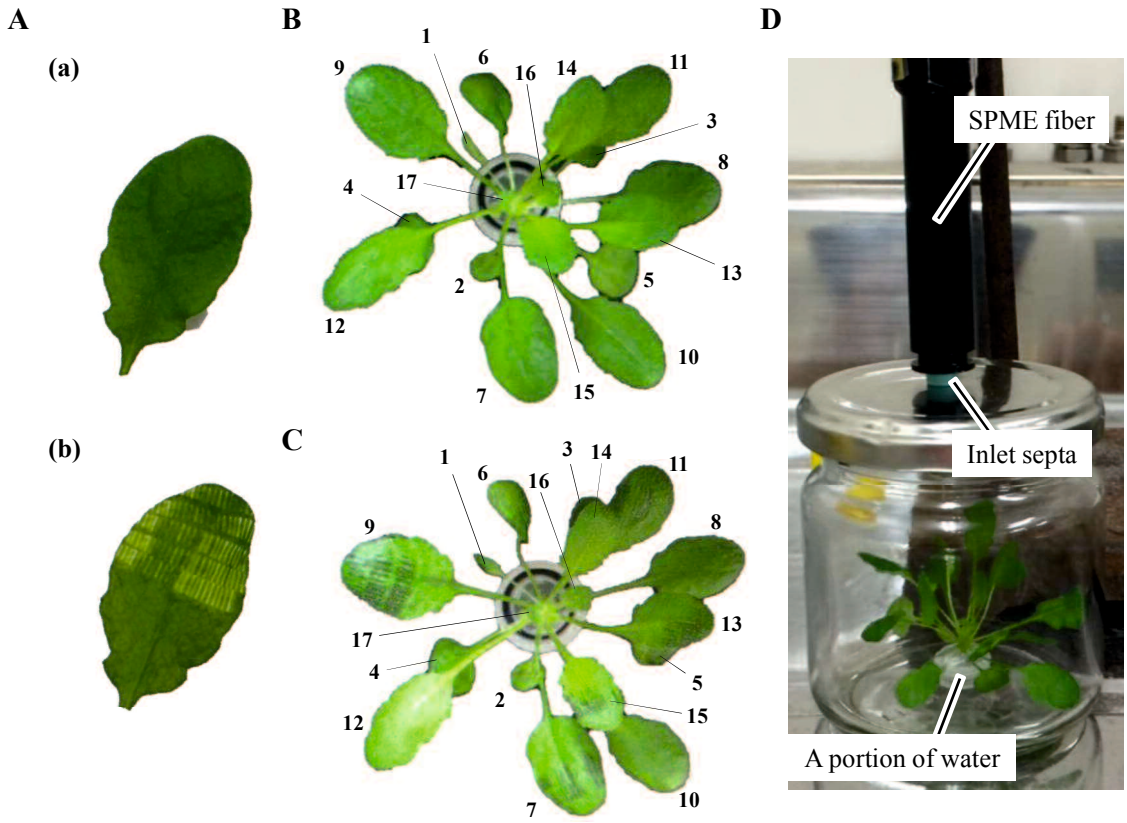

Fig. 13. Leaves after mechanical wounding. A, About 20% of apical part of Arabidopsis leaf was wounded by pinching with forceps. (a); leaf before wounding, (b); after wounding. B, Numbering of leaf (from the oldest to the youngest). C, After cutting at the hypocotyl close to junction between hypocotyl and root, the above-ground part of Arabidopsis was placed on the cap of vial (Micro tube 2 mL, 72.693, SARSTEDT, Tokyo, Japan) filled with tap water, then odd numbered leaves were wounded. D, The above-ground parts of Arabidopsis plants with cap were immediately placed into a glass jar (187 mL, 67 mm diameter, 75 mm height). A SPME fiber was exposed to the headspace immediately after placing the plants in the jar, and collection time was 30 min under the light.

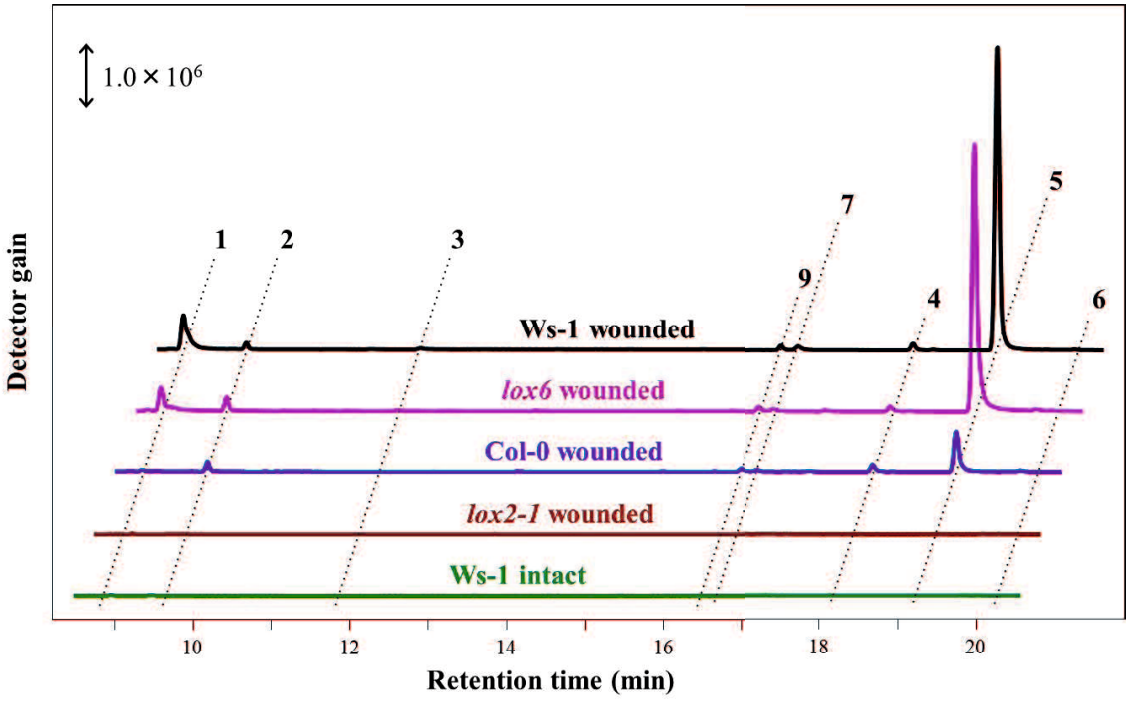

Fig. 14. Headspace volatiles formed from partially wounded Arabidopsis leaves. Representative chromatograms were shown (black: Ws-1 wounded, pink: *lox6* wounded, blue: Col-0 wounded, brown: *lox2-1* wounded, and green: Ws-1 intact).

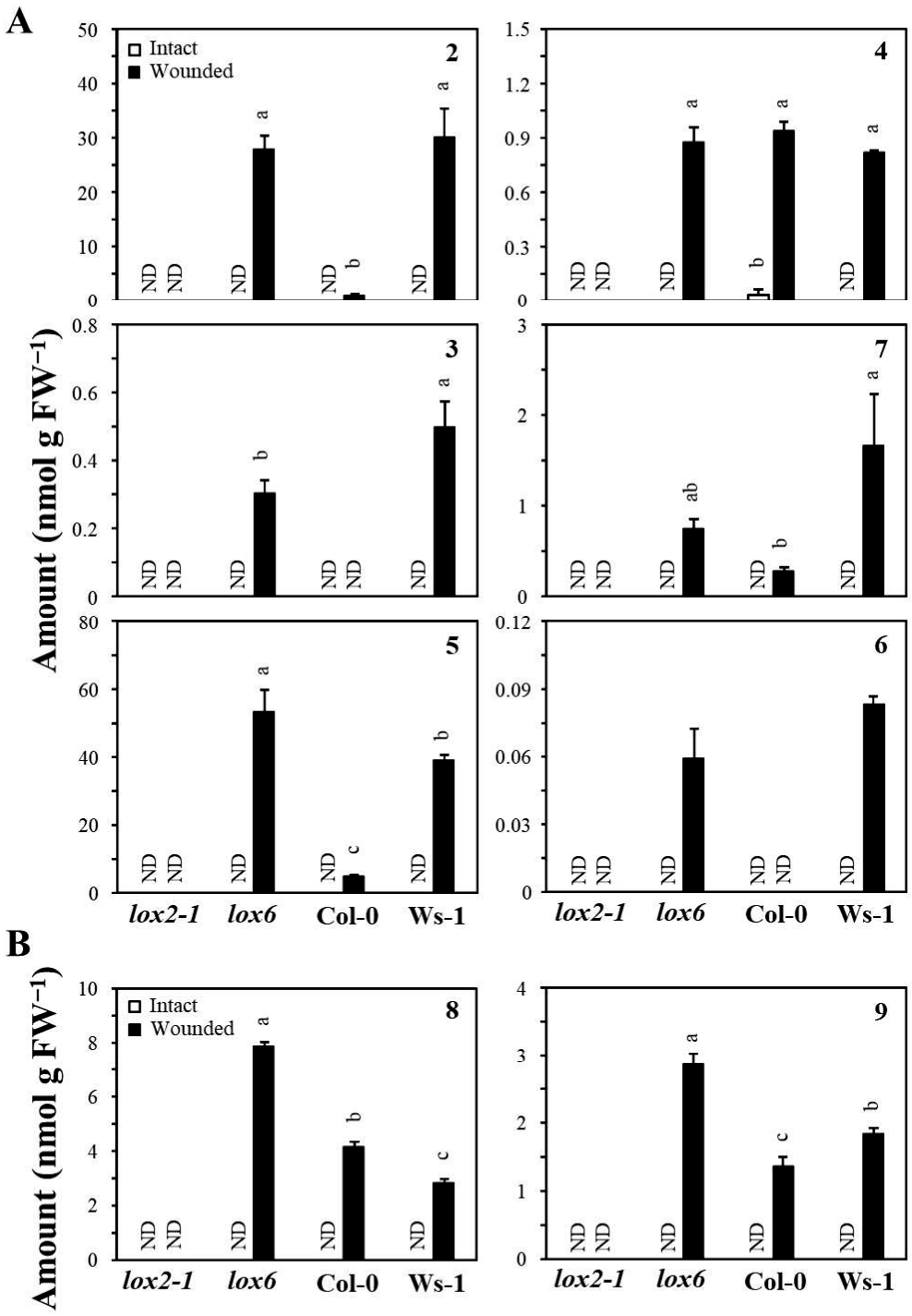

Fig. 15. LOX2 is involved in the emission of GLVs and C5 volatiles from Arabidopsis leaves upon mechanical wounding. A, the amount of GLVs formed from intact and wounded leaves of each Arabidopsis line. B, the amount of C5 volatile compounds formed from intact and wounded leaves of each Arabidopsis line. Mean values ± SEM (error bars) are shown (n = 3, biological replicates). Different letters show significant difference (two-way ANOVA, Tukey, $P < 0.05$). ND, not detected. Note that **1** was detected in all lines, but it was not appropriate to quantification because it highly contaminated from atmosphere.

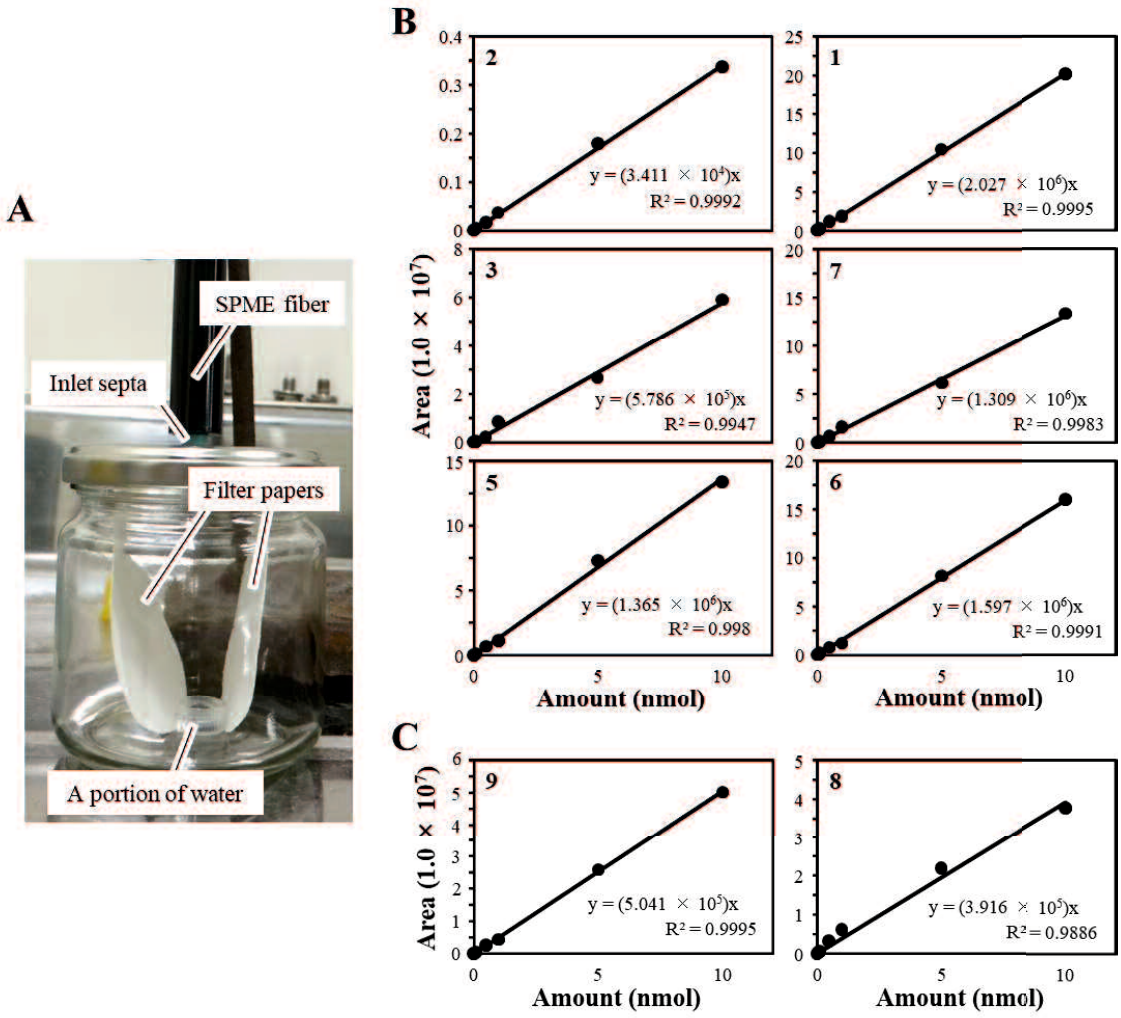

Fig. 16. Calibration curves used for the quantification of GLVs and C5 volatiles. A, Two sheets of filter paper infiltrated with 150 μL of the volatile-suspension were placed inside of the jar to give almost similar surface area with plant leaves. B, Calibration curves for GLVs. C, Calibration curves for C5 volatile compounds.

Time course of volatile formation after freeze-thaw treatment

The results shown above indicated that LOX2 was essential to the formation of both GLVs and C5 volatiles. The amounts of GLVs in intact leaf tissues were low, but freeze-thaw tissue-disruption resulted in 'burst' of their formation. On the contrary, the substantial amounts of C5 volatiles were detected in intact tissues, and freeze-thaw tissue-disruption caused little changes in their amounts. This suggested that the biosynthetic pathways to form GLVs and C5 volatile compounds, both of which were facilitated by LOX2 activity, were differently regulated. In order to know how differently the two pathways were controlled, I carried out the time course analysis on GLVs and C5 volatiles after freeze-thaw tissue-disruption (Fig. 17).

In intact leaf tissues of Ws-1, substantial levels of **2**, **3**, and **1** were detected. Upon tissue disruption, **2** was rapidly formed and its level met a peak at 3 min after disruption, and thereafter, the amount gradually decreased. Compound **3** and **5** were gradually formed and their highest levels were observed at 30 to 60 min after tissue disruption, and thereafter, their levels were almost constant. Compound **1** was also rapidly formed by 3 to 5 min after tissue disruption and its amount was kept largely constant thereafter. The amounts of GLVs in intact tissues of *lox2-1* mutant were quite low, and showed little changes after freeze-thaw tissue-disruption (Fig. 18A). At 30 min after freeze-thaw treatment, detectable increase in **2** was found.

A slight increase in the amounts of C5 volatiles was detected after tissue disruption of Ws-1 leaves. After meeting small peaks at 3 min with **8** and **9** and at 10 to 30 min with **10**, their amounts were almost constant. *lox2-1* mutant had undetectable levels of **8** and **9** in intact tissues, but their amounts slowly increased after freeze-thaw treatment. Compound **10** showed quite different kinetics from the other two C5 volatiles. Its level in intact *lox2-1* leaves was similar with that in Ws-1, and slightly increased after tissue disruption to meet a peak at 10 min with the amount higher than that in Ws-1; thereafter, its level gradually decreased to that found in Ws-1 leaves (Fig. 18B).

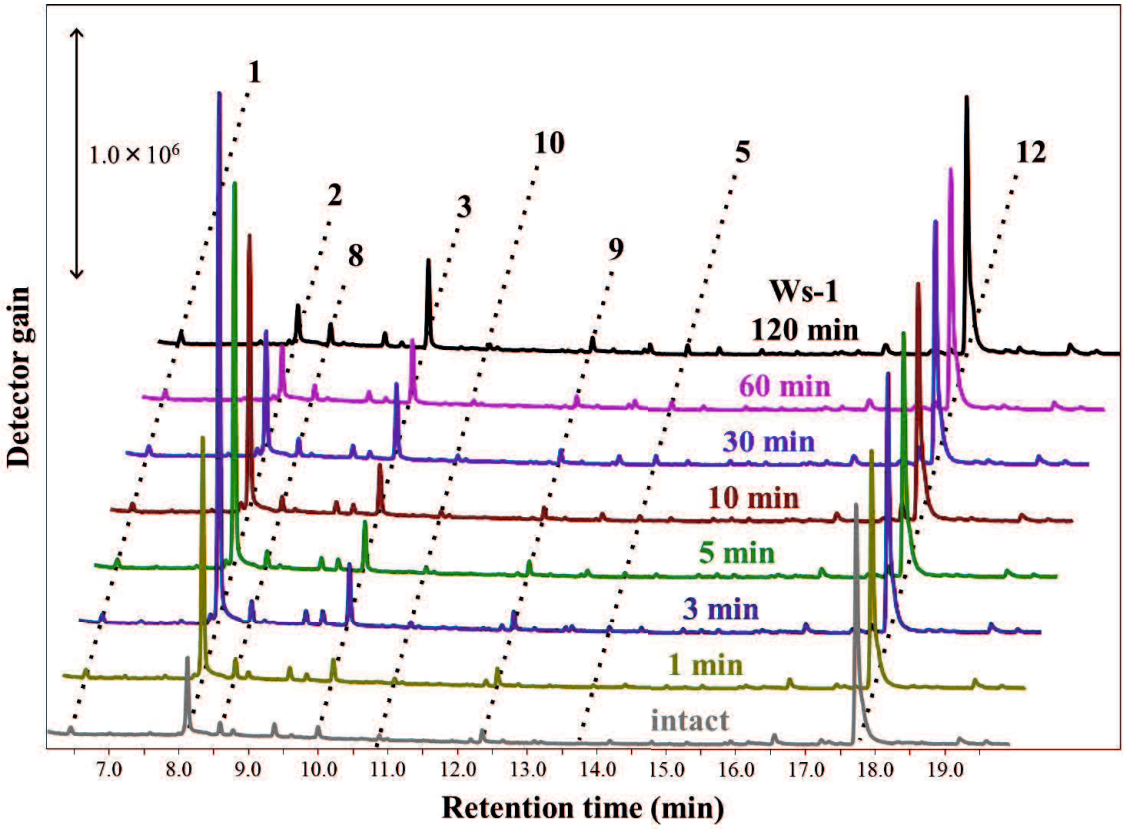

Fig. 17. Volatiles formed after freeze-thaw treatment on Arabidopsis leaves. Freeze-thaw treatment was carried out in closed glass vial and subsequently incubated at 25°C for a given time. Representative chromatograms of freeze-thaw treated Ws-1 were shown (black: 120 min, pink: 60 min, sky blue: 30 min, brown: 10 min, green: 5 min, blue: 3 min, yellow: 1 min, and gray: intact). 12, *n*-nonan-1-yl acetate (IS).

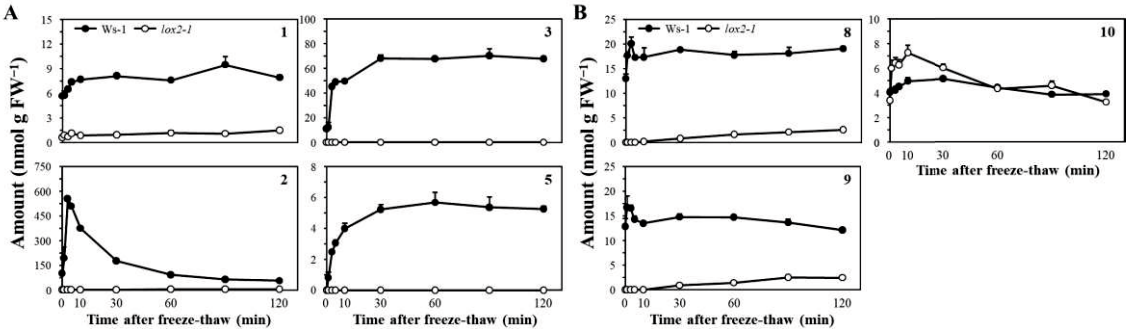

C

Line	Time after freeze-thaw (min)	GLVs (nmol g FW⁻¹) 1	2	3	5
lox2-1	0 (intact)	0.61 ± 0.13 ^{d}	ND	ND	ND
	1	0.90 ± 0.19 ^{d}	ND	ND	ND
	3	0.69 ± 0.02 ^{d}	ND	ND	ND
	5	1.09 ± 0.08 ^{d}	ND	ND	ND
	10	0.85 ± 0.03 ^{d}	ND	ND	ND
	30	0.93 ± 0.22 ^{d}	1.04 ± 0.13 ^{f}	ND	ND
	60	1.15 ± 0.26 ^{d}	1.17 ± 0.09 ^{f}	ND	ND
	90	1.06 ± 0.09 ^{d}	1.84 ± 0.14 ^{f}	ND	ND
	120	1.46 ± 0.13 ^{d}	2.44 ± 0.23 ^{f}	ND	ND
Ws-1	0 (intact)	5.64 ± 0.07 ^{c}	100 ± 5.77 ^{de}	11.0 ± 1.35 ^{c}	ND
	1	5.72 ± 0.58 ^{c}	193 ± 68.3 ^{c}	12.2 ± 3.83 ^{c}	0.81 ± 0.36 ^{e}
	3	6.47 ± 0.16 ^{bc}	554 ± 13.9 ^{a}	45.2 ± 0.96 ^{b}	2.47 ± 0.06 ^{d}
	5	7.37 ± 0.12 ^{b}	509 ± 6.05 ^{a}	49.1 ± 0.76 ^{b}	3.04 ± 0.21 ^{cd}
	10	7.67 ± 0.27 ^{b}	374 ± 3.70 ^{b}	49.7 ± 0.58 ^{b}	3.97 ± 0.37 ^{bc}
	30	8.10 ± 0.12 ^{ab}	175 ± 5.70 ^{cd}	68.1 ± 2.82 ^{a}	5.22 ± 0.33 ^{ab}
	60	7.58 ± 0.10 ^{b}	91.3 ± 5.11 ^{de}	67.7 ± 1.59 ^{a}	5.66 ± 0.65 ^{a}
	90	9.47 ± 0.97 ^{a}	63.3 ± 1.36 ^{ef}	70.3 ± 5.59 ^{a}	5.35 ± 0.67 ^{ab}
	120	7.91 ± 0.27 ^{ab}	55.8 ± 2.73 ^{ef}	67.84 ± 1.84 ^{a}	5.24 ± 0.20 ^{ab}

D

Line	Time after freeze-thaw (min)	C5 volatiles (nmol g FW⁻¹) 8	9	10
lox2-1	0 (intact)	ND	ND	3.38 ± 0.55 ^{fg}
	1	ND	ND	5.99 ± 0.67 ^{abcde}
	3	ND	ND	6.42 ± 0.43 ^{ab}
	5	ND	ND	6.27 ± 0.43 ^{abc}
	10	0.15 ± 0.08 ^{c}	ND	7.26 ± 0.61 ^{a}
	30	0.77 ± 0.21 ^{c}	0.95 ± 0.01 ^{c}	6.03 ± 0.28 ^{abcd}
	60	1.60 ± 0.36 ^{c}	1.44 ± 0.31 ^{c}	4.33 ± 0.30 ^{defg}
	90	2.07 ± 0.30 ^{c}	2.56 ± 0.38 ^{c}	4.58 ± 0.36 ^{cdefg}
	120	2.59 ± 0.41^{c}	2.47 ± 0.24 ^{c}	3.24 ± 0.06 ^{g}
Ws-1	0 (intact)	12.96 ± 0.97 ^{b}	12.89 ± 1.57 ^{ab}	4.05 ± 0.23 ^{fg}
	1	17.64 ± 0.76 ^{a}	16.68 ± 2.31 ^{a}	4.20 ± 0.12 ^{efg}
	3	20.05 ± 1.34 ^{a}	16.55 ± 0.61 ^{a}	4.20 ± 0.32 ^{efg}
	5	17.23 ± 0.30 ^{a}	14.29 ± 0.65 ^{ab}	4.50 ± 0.02 ^{cdefg}
	10	17.27 ± 1.92 ^{a}	13.51 ± 0.44 ^{ab}	4.96 ± 0.28 ^{bcdefg}
	30	18.79 ± 0.37 ^{a}	14.74 ± 0.66 ^{ab}	5.14 ± 0.11 ^{bcdef}
	60	17.71 ± 0.73 ^{a}	14.69 ± 0.54 ^{ab}	4.43 ± 0.12 ^{defg}
	90	18.04 ± 1.28 ^{a}	13.64 ± 0.66 ^{ab}	3.87 ± 0.13 ^{fg}
	120	19.01 ± 0.54 ^{a}	12.10 ± 0.28 ^{b}	3.90 ± 0.06 ^{fg}

Fig. 18. Time course of formation of GLVs and C5 volatile compounds in Arabidopsis leaves after freeze-thaw treatment. A, the amount of GLVs in intact and freeze-thaw treated lines. B, the amount of C5 volatile compounds in intact and freeze-thaw treated lines. Closed circle indicates Ws-1 and open circle indicates *lox2-1*. Mean values ± SEM (error bars) are shown (n = 3, technical replicates). C, The amount of GLVs. D, The amount of C5 volatiles. In **9**, there is significant difference in genotype (Ws-1 and *lox2-1*) and in interaction effect between genotype and treatment (time after freeze-thaw, 0 min to 120 min) (two-way ANOVA, Tukey, $P < 0.01$), but no significant difference in treatment.

Discussion

Lipoxygenases (LOXs) are the enzymes that catalyze oxygenation of polyunsaturated fatty acids to form corresponding fatty acid hydroperoxides. Acyl groups in glycerolipids are also oxygenated to form corresponding lipid hydroperoxides by some of LOXs [32]. The hydroperoxides are in most cases further metabolized to yield a wide range of bioactive compounds called oxylipins. LOXs are found in animals, plants, fungi, and even in some of prokaryotes, and these organisms have abilities to form bioactive oxylipins [2]. Most plants have several to dozens of LOX isoforms, probably because plants should employ distinct oxylipin-biosynthetic pathway to form respective bioactive compound that exerts its function in a defined tissues and/or at a defined timing [1]. GLVs and JAs are the bioactive oxylipins extensively studied so far in plants [5]. With potatoes, *N. attenuata*, tomatoes, rice, and maize, a specific LOX that is specifically involved in either the GLV pathway or the JA pathway has been reported even though a partial overlap of one LOX isoform in the two pathways was also evident especially in tomatoes and rice [7–10,12,14]. Arabidopsis has six *LOX* genes, *AtLOX1–6*, and this study indicates that LOX2 is essential to formation of GLVs as well as C5 volatiles. None of the other LOXs is involved in the formation of oxylipin volatiles. AtLOX2 is the major JA-producing LOX in Arabidopsis leaves [25], thus, apparently, one LOX isoform in Arabidopsis, AtLOX2, is essential to both GLV formation and JA formation.

It has been proposed that GLV-specific and JA-specific LOXs could be clustered into two clades in the phylogenetic tree based on their amino acid sequences. However, the clustering is not so clear, and, for example, OsHI-LOX locates in the GLVs associated LOX cluster even though OsHI-LOX is JA-associated (Fig. 19). The situation with OsLOX1 (LOX-L1) is more complicated. OsLOX1 (LOX-L1) is in the 9-LOX clade, but it has both of 9-LOX and 13-LOX activity, moreover, it is involved in both the GLV and JA pathways [14]. In the phylogenetic tree, AtLOX2 locates in the GLV-associated LOX cluster where GLV-associated LOXs, such as TomloxC, StLOX2 (LOX-H1), NaLOX2 and ZmLOX10, locate among the other uncharacterized LOXs. As shown here, AtLOX2 is a LOX associated with both GLV and JA. The other three 13-LOXs found Arabidopsis, AtLOX3, AtLOX4, and AtLOX6, are JA-associated LOX [15]. Accordingly, clustering LOXs based on their specific involvement in GLV or JA biosynthetic pathway is inappropriate at least with Arabidopsis. It is assumed that the function of each LOX isoform was acquired after diverging each isoform. Further accumulation of the knowledge on the function of each LOX isoform in the other plant species is essential to elucidate how plants allocated the function of LOX during evolution.

Mechanical wounding on plant leaves resulted in disruption of cells, which causes the GLV-burst as found in this study with freeze-thaw treated, completely disrupted leaf tissues. I confirmed that LOX2 was essential to support the GLV-burst through serving hydroperoxides of galactolipids and linolenic acid to HPL in the disrupted tissues. This happened within 3 min after tissue disruption as noted with the time course of **2** formation. A portion of **2** thus formed was subsequently converted into **3** through isomerization or into **5** through reduction. At the same time, another portion of hydroperoxides of galactolipids formed by LOX2 action was converted to yield

arabidopsides by AOS [25,27,33]. This 'arabidopside-burst' was evident as fast as 15 min after mechanical wounding [34]. Because spatial compartmentalization was almost completely abolished in disrupted tissues, the fates of hydroperoxides formed by LOX2 should be uncontrollable and might be dependent on the relative activities of enzymes that converted the hydroperoxides. In fact, HPL and AOS somewhat competed for the same substrates in disrupted Arabidopsis leaf tissues [27]. Therefore, it is assumed that tissue-disruption quickly accelerates LOX2 action to form hydroperoxides of galactolipids and fatty acids, and the hydroperoxides are converted into **2** and its counterparts, i.e., free and esterified forms of traumatin and its derivatives, or into arabidopsides and OPDA largely dependent on the availability of HPL and AOS in the disrupted tissues.

It must be noticed that LOX2 catalyzes its reaction even in intact leaf tissues because substantial amounts of C6-aldehydes and C5 volatiles were found in intact tissues. LOX2 is the sole enzyme supplying the hydroperoxide intermediates to the volatile formation other than **1** and **10**. The amount of **10** formed by any of the mutant lines was not different from the wild type ecotypes; therefore, the volatile formation was independent on LOX-mediated oxygenation of lipids and fatty acids. It is suggested that LOX2 exerted its catalytic activity in two totally different situations; one in intact cells and the other in disrupted cells. Because it is unlikely that the amount of LOX2 protein increases in disrupted tissues through induction of *LOX2* gene expression, there must be a mechanism that suppresses or activates the LOX2 reaction in the intact or disrupted tissues.

Remarkably, upon disorganization of cell architecture caused by tissue disruption, LOX2 is quickly and extensively activated to form GLVs with the aid of HPL and esterified/free OPDA with the aid of AOS. Because the amounts of C5 volatiles that were formed through radical reaction on the hydroperoxides formed by LOX2 showed only a little increase after tissue disruption, the hydroperoxides formed should be instantly served to HPL and AOS with avoiding spontaneous homolytic degradation or side reaction mediated by LOX2 [8] (Fig. 20). The GLV-burst is largely supported by enhanced reaction of LOX2 that takes place within 3 min, while in intact cells LOX2 activity should be extensively low. Because LOX2 is one of major stromal enzymes accounting to 0.75% of total stromal proteins found in plastids of Arabidopsis [35] and galactolipids abundant in thylakoid membranes are the substrates of LOX2, there must be a system to suppress its activity in intact cells, which is rapidly released when the cells would be disrupted.

Human LOXs have attracted a lot of interests because the enzyme activities are linked with various diseases [36], and it is known that some of human LOX enzymes are activated by various factors, including Ca^{2+}, accompanying protein such as 5-LOX activating protein, or lipid compounds [37]. By now, little is known about the mechanism that regulates the activity of plant LOX enzymes. The finding shown here indicated that activity of Arabidopsis LOX2 is largely suppressed in intact plastids, but upon disruption of the plastids, the suppression was instantly released to support GLV-burst. The mechanism to control activity of Arabidopsis LOX2 was investigated in the next Chapter.

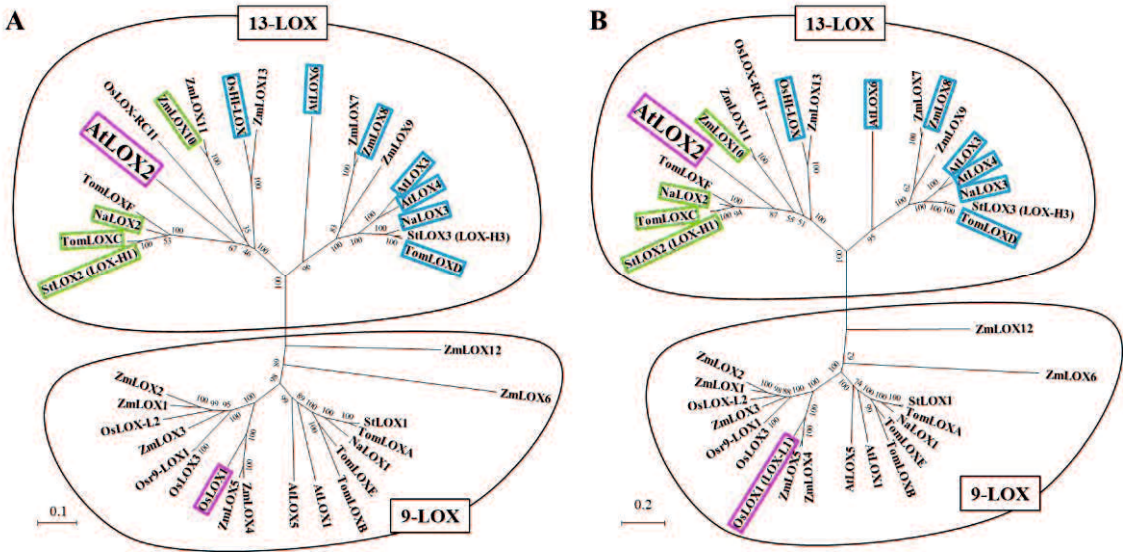

Fig. 19. Phylogenetic analysis of LOXs from different plant species. A phylogenetic analysis was carried out in MEGA6 using Neighbor-joining method (A) and Maximum Likelihood method (B) based on each LG model + G + I (8 categories). The scale bars represent 0.1 and 0.2 amino acid substitutions per site, respectively. Taxon labels are depicted in pink for the 13-LOX clade, in gray for 9-LOX clade. GLV-specific LOX is denoted in green, JA-specific LOX is denoted in blue, and both GLV-, JA-specific LOX is denoted in magenta. OsLOX1 forms both 9- and 13-hydroperoxide [14].

Plant species	Gene	Accession number
Arabidopsis thaliana	*AtLOX1*	Q06327
	AtLOX2	P38418
	AtLOX3	Q9LNR3
	AtLOX4	Q9FNX8
	AtLOX5	Q9LUW0
	AtLOX6	Q9CAG3
Nicotiana attenuata	*NaLOX1*	AAP83136
	NaLOX2	AAP83137
	NaLOX3	AAP83138
Oryza sativa	*OsHI-LOX*	BAF24113
	OsLOX1	ABD47523
	OsLOX3	BAS85907
	OsLOX-L2	CAA45738
	OsLOX-RCI1	CAC01439
	Osr9-LOX1	BAD02945
Solanum lycopersicum	*TomLOXA*	P38415
	TomLOXB	P38416
	TomLOXC	AAB65766
	TomLOXD	AAB65767
	TomLOXE	AAG21691
	TomLOXF	ACM77790
Solanum tuberosum	*StLOX1*	P37831
	StLOX2 (LOX-H1)	CAA65268
	StLOX3 (LOX-H3)	CAA65269
Zea mays	*ZmLOX1*	AAF76207
	ZmLOX2	ABC59686
	ZmLOX3	DAA50837
	ZmLOX4	ABC59687
	ZmLOX5	ABC59688
	ZmLOX6	ABC59689
	ZmLOX7	ABC59690
	ZmLOX8	ABC59691
	ZmLOX9	ABC59692
	ZmLOX10	ABC59693
	ZmLOX11	ABC59694
	ZmLOX12	ABC59695
	ZmLOX13	DAA47969

Table. 2. Genbank accession numbers of each LOX proteins used for phylogenetic analysis.

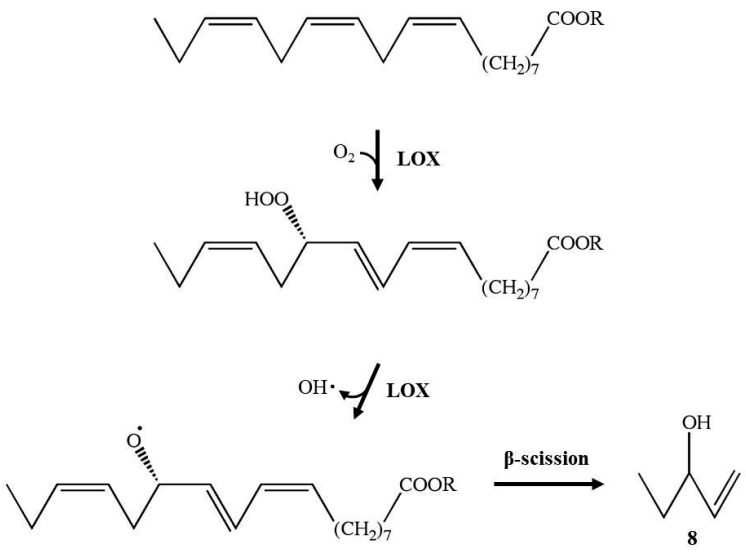

Fig. 20. The biosynthetic pathway of C5 volatiles. It is proposed that C5 volatiles are formed from 13-HPOT followed by a β-scission [8]. LOX reactions generate an alkoxyl radical, which would undergo non-enzymatic cleavage to generate C5 alcohols.

CHAPTER TWO

Involvement of Ca^{2+}-dependent activation of lipoxygenase in green leaf volatile-burst in *Arabidopsis thaliana*

Introduction

A real-time repulsion of actively infesting herbivores and prevention of invasion of pathogens into plant tissues through open wounds made by herbivores or mechanical damage require immediate formation of green leaf volatiles (GLVs) at the site of damage. Prompt formation of GLVs is also critical in facilitating indirect defense through relaying timely information about herbivores actively infesting plant tissues to their natural enemies (parasites and carnivores) [4]. Because it is unlikely that damaged plant tissues can adequately fortify a biosynthetic pathway by upregulating transcription within seconds, the activation of enzymes as opposed to an increase in enzyme amounts for GLVs formation should be involved. However, the mechanism of GLV-burst has not been completely addressed yet [4,38–40].

The synthesis of leukotrienes, which are a family of oxylipins in animal cells, is tightly regulated by 5-lipoxygenase (5-LOX) activity, as one of the activities responsible for key regulatory steps [41]. In resting cells, 5-LOX is a soluble enzyme, but external stimuli activate signaling events that translocate 5-LOX onto nuclear membranes, where its substrate, arachidonic acid, is available. For the translocation process, association of 5-LOX with Ca^{2+} is essential [41,42]. 5-LOX enzyme consists of an N-terminal β-barrel domain and a C-terminal catalytic domain. The N-terminal β-barrel domain is also termed as a C2-like domain or a PLAT (polycystin-1, lipoxygenase and alpha toxin) domain. Asn43, Asp44, and Glu46 situated in loop 2 of the 5-LOX PLAT domain are believed to be the Ca^{2+} binding ligands [43]. After binding Ca^{2+}, the hydrophobicity of 5-LOX increases, this facilitates translocation of 5-LOX onto the nuclear membrane [41–43]. Plant LOXs also consist of an N-terminal PLAT and C-terminal catalytic domains. Association of Ca^{2+} with the N-terminal PLAT domain has been reported to cause translocation onto membranes with several plant LOXs, such as soybean seed LOX-1 [44] or maize LOX1 [45]. The analogies between animal and plant LOXs lead me to assume that Ca^{2+} plays a role in GLV-burst through the activation of LOX after injury or stress to plant tissues.

Ca^{2+} homeostasis in plant cells is tightly regulated. The most abundant Ca^{2+} store in plant cells is vacuoles, and Ca^{2+} concentrations in vacuoles range from 0.2–5 mM [46]. Conversely, chloroplast stroma has <150 nM of free Ca^{2+}, similar to that in cytosol [47]. It is suggested that several biotic/abiotic stimuli cause the influx of Ca^{2+} into stroma. For example, a shift from light to dark conditions stimulates stomatal Ca^{2+} influx [48]. Wounding also triggers Ca^{2+} influx into cytosol [49]. Such stimuli also activate the production of GLVs [4,22,38,39,50], which further prompted us to investigate the relationship between Ca^{2+} and plant LOX activity and its effect on GLV-burst.

In Arabidopsis, AtLOX2 is almost exclusively involved in GLV-burst (described in Chapter 1, Fig. 7). AtLOX2 is localized in chloroplast stroma and accounts for 0.75% of the total stromal proteins in resting cells [35]. Monogalactosyldiacylglycerol (MGDG), which is abundant in the thylakoid membrane, is the substrate for AtLOX2 required for the formation of GLVs [27]. Consequently, there must be mechanisms for suppressing spontaneous reactions between MGDGs in thylakoid membranes and AtLOX2 in chloroplast stroma of unstimulated plant cells, and to activate

AtLOX2 within seconds after the perception of appropriate stimuli. In the present study, I confirmed the key role of AtLOX2 in GLV-burst and examined the effects of Ca^{2+}-specific chelating agents on AtLOX2 activity and GLV-burst in Arabidopsis leaves.

Materials and Methods

Plant materials

Arabidopsis thaliana *lox2-1* mutants (provided by Prof. Dr. Edward E. Farmer, University of Lausanne, Switzerland) were backcrossed twice with Ws-1 (described in Chapter 1, materials and methods). Arabidopsis were grown at 22°C under 10 h of light (50–150 μmol m^{-2} s^{-1}) a day for 42–56 days. *Solanum lycopersicum* cv. M82 (provided by Prof. Dr. Harry J. Klee, University of Florida, USA), *Nicotiana attenuate* (provided by Prof. Dr. Ian T. Baldwin, Max Planck Institute, Germany), *Oryza sativa* ssp. *japonica* cv. Nipponbare (provided by Prof. Dr. Toshihiro Kumamaru, Kusyu University, Japan), *Glycine max* cv. Fukuyutaka and *Trifolium repens* (commercially obtained from Nakayama Daikichi Shoten, Kumamoto, Japan, and KANEKO SEEDS, Gunma, Japan, respectively) were grown at 25°C under 14 h of light (50–150 μmol m^{-2} s^{-1}) a day. Expanded leaves (41–48 days-old tomato and tobacco, 24–31 days-old clover and rice, 14–28 days-old soybean and maize) were cut off with razor blade and immediately used for experiments after weighing.

Analysis of MGDG-OOHs

Arabidopsis leaves (Col-0, 100 mg fresh weight) were disrupted with 2 mL of 50 mM MES-KOH, pH 6.3 for 1 min with a mortar and pestle. After the addition of 5 μL of 1 mM formononetin in methanol as an internal standard, 7.5 mL of chloroform ($CHCl_3$)/methanol (1:2, v/v) containing 0.1% butylated hydroxytoluene was added and the solution was mixed vigorously. After the addition of 2.5 mL of $CHCl_3$ and 1% (w/v) KCl to the mixture, the aqueous and organic phases were separated by centrifugation at 300 × g for 5 min at 25°C. The aqueous phase was re-extracted with 2 mL $CHCl_3$, and the combined organic phase was washed with 2 mL of 1% (w/v) KCl. The hydroperoxides (OOHs) were reduced by adding 100 μL of 0.1 M triphenylphosphine (TPP) in *n*-hexane to the extract, followed by incubation for 15 min at 25°C. The solvent was dried under a vacuum, and the residue was dissolved in 100 μL of acetonitrile. A portion (4 μL) of the extract was subjected to a high performance liquid chromatography-photodiode array detector-MS/MS system [51] after filtration through a DISMIC-03JP (0.5 μm, ADVANTEC Toyo Roshi Kaisha, Ltd., Tokyo, Japan) filter. Lipid-OOHs were separated on a Mightysil RP-18 column (150 × 2 mm inner diameter, Kanto Chemical, Tokyo, Japan) with a binary gradient consisting of water/formic acid (100:0.1, v/v, solvent A) and acetonitrile/formic acid (100:0.1, v/v, solvent B). For *O*-[13-hydroxy-(9*Z*,11*E*,15*Z*)-9,11,15-octadecatrienoyl]-*O*-[11-hydroxy-(7*Z*,9*E*,13*Z*)-7,9,13-hexadecatrienoyl]-MGDG (MGDG-13-HOT/11-HHT) and *O*-[13-hydroxy-(9*Z*,11*E*,15*Z*)-9,11,15-octadecatrienoyl]-*O*-[(7*Z*,10*Z*,13*Z*)-7,10,13-hexadecatrienoyl]-MGDG (MGDG-13-HOT/C16:3), the run consisted of a linear increase from 20% B to 95% B over 60 min (flow rate, 0.2 mL min^{-1}). For bis-*O*-[13-hydroxy-(9*Z*,11*E*,15*Z*)-9,11,15-octadecatrienoyl]-MGDG (MGDG-bis-13-HOT), the run consisted of a linear increase from 50% B to 60% B over 60 min, held for 10 min and increased to 95% B over 30 min (flow rate, 0.2 mL min^{-1}). *O*-[13*S*-hydroperoxy-(9*Z*,11*E*,15*Z*)-9,11,15-octadecatrienoyl]-*O*-[11*S*-hydroperoxy-(7*Z*,9*E*,13*Z*)-7,9,13-hexadecatrienoyl]-MGDG (MGDG-13-HPOT/11-HPHT) was prepared from MGDG-C18:3/C16:3, *O*-[(9*Z*,12*Z*,15*Z*)-9,12,15-octadecatrienoyl]-*O*-[(7*Z*,10*Z*,13*Z*)-7,10,13-hexadecatrienoyl]-MGDG (MGDG-C18:3/C16:3) purified from spinach leaves with soybean seed LOX-1 as described by Nakashima et al. [27]. Quantification was done by reading absorbance at 234 nm with a molecular coefficient (ε) of 25,000 M^{-1} cm^{-1} for 1-hydro(pero)xy-2,4-pentadien moiety.

Analysis of volatiles

Arabidopsis leaves (100 mg fresh weight) were disrupted with 2 mL of 50 mM MES-KOH, pH 6.3 supplemented with/without 1 mM BAPTA (Toronto Research Chemicals, North York, Canada) or EGTA (Dojindo Laboratories, Kumamoto, Japan) for 3 min with a mortar and pestle. Enzyme reactions were terminated by the addition of 2 mL of methyl *tert*-butyl ether, and extraction and analysis of GLVs were carried out using GC-MS as described in Chapter 1, materials and methods, but without incubation for 10 min at 60°C.

Hydroperoxide lyase (HPL) activity assay

Arabidopsis *lox2-1* mutant leaves (200 mg) were homogenized with 400 μL of 50 mM MES-KOH pH 6.3 for 3 min with a mortar and pestle. Homogenate was used as crude enzyme. A portion of crude enzyme (100 μL) was mixed with 90 μL of 10 mM BAPTA in 50 mM MES-KOH pH 6.3, then 10 μL of 5 mM 13-HPOT, prepared from α-linolenic acid (LNA, Sigma-Aldrich, St. Louis, MO, USA) with soybean LOX [31], in ethanol was added. After 3 min incubation, formed volatile compounds was extracted and analyzed (described in Chapter 1, materials and methods).

LNA analysis

Arabidopsis (100 mg) were homogenized with 2 mL of 50 mM MES-KOH pH 6.3 containing 10 mM BAPTA for 3 min with a mortar and pestle. Homogenate was acidified to pH 4.0 by adding $HClO_4$, and 50 μL of 0.2 μg mL^{-1} margaric acid (Tokyo Chemical Industry, Tokyo, Japan) was added as internal standard. $CHCl_3$/methanol (1:2, v/v, 7.5 mL) was subsequently added and mixed vigorously. After addition of 2.5 mL of $CHCl_3$ and 2.5 mL of 0.1 M KCl to the mixture, the aqueous and organic phases were allowed to separate. The aqueous phase was re-extracted with 2 mL of $CHCl_3$, and the combined organic phase was washed with 2 mL of 0.1 M KCl. The solvent was dried up under vacuum, and the remaining residue was dissolved in 150 μL of diethyl ether. After addition of CH_2N_2 (prepared by the reaction of *N*-methyl-*N'*-nitro-*N*-nitrosoguanidine with sodium hydroxide) in MTBE, solvent was incubated 25°C for 5 min. The solvent was re-dried up under vacuum, and the remaining residue was dissolved in 100 μL of *n*-hexane. A portion (1 μL) was subjected to GC/MS described in Chapter 1. Injection was carried out with split ratio of 1:3 at 240°C. The oven temperature was 190°C with isocratic mode.

3D-model construction

Arabidopsis LOX2 (P38418, UniProt), tomato LOXC (Q96573, UniProt), and tobacco LOX2 (Q6X5R6, UniProt) models without an estimated transit peptide (56, 42, and 63 amino acids in N-terminal, respectively) were constructed with SWISS-MODEL workspace [52] based on soybean seed LOX-1 (PDB, 3PZW). Images of the structures with coral 8*R*-LOX (PDB, 2FNQ) [53] and human 5-LOX (PDB, 3O8Y) [42] were generated using PyMOL (DeLano Scientific, Palo Alto, CA, USA).

Statistics

All values are presented as means ± SEM. Statistical analyses were performed with BellCurve in Microsoft Excel (Social Survey Research Information Co., Tokyo, Japan). Statistical methods used are described in the captions of figures.

Results

Detection of MGDG-OOHs from Arabidopsis leaves

A previous study showed that a large proportion of GLVs were formed without the lipid-hydrolyzing step and that the first committed step of GLV biosynthesis in Arabidopsis was largely at the oxygenation of acyl groups of lipids by LOX [27]. AtLOX2 was the LOX that was almost exclusively responsible for GLVs formation in Arabidopsis leaves (described in Chapter 1, Fig. 7). Accordingly, we assumed that AtLOX2 activity played a key role in GLV-burst. First, we examined properties of recombinant AtLOX2 expressed with *E. coli*, but recombinant AtLOX2 were too unstable to obtain reliable results. Consequently, we evaluated *ex vivo* AtLOX2 activity to form OOHs from endogenous substrates in disrupted Arabidopsis leaves.

Arabidopsis Col-0 is a natural variant deficient in hydroperoxide lyase (HPL) activity because of 10-bp deletion in the open reading frame of the *HPL* gene [28]. Accordingly, LOX2 products, i.e., galactolipid-OOHs, accumulate in the disrupted leaf tissues in Col-0. When crude lipid extracts prepared from disrupted Arabidopsis leaf tissues were analyzed using LC-MS/MS, three distinct peaks with diagnostic features of MGDG-OOHs, i.e., spectra with absorption maximum at 234 nm and $[M-H]^-$ values corresponding to MGDG-O(O)Hs formed from either MGDG-C18:3/C16:3 or MGDG-C18:3/C18:3, were detected (Fig. 21). The major compound was identified as MGDG-13-HOT/11-HHT by comparing its retention time, absorption spectrum, and MS/MS profiles with those of an authentic standard after reduction with TPP. The other peaks were tentatively assigned as MGDG-13-HOT/C16:3 and MGDG-bis-13-HOT based on their absorption spectra and MS/MS profiles (Fig. 21).

MGDG-OOHs were not detected in intact Arabidopsis leaves; however, increased amount of MGDG-OOHs was detected 1 min after complete disruption of Arabidopsis leaves (Fig. 22). The concentration of MGDG-OOHs reached up to 171 nmol g FW^{-1} (corresponding to 305 nmol g FW^{-1} of acyl groups with OOH), which accounted for 90.2% of the amount of (*Z*)-3-hexenal found in disrupted Arabidopsis Ws-1 leaves (Fig. 24). My attempts to detect OOHs of digalactosyldiacylglycerol (DGDG), sulfoquinovosyldiacylglycerol (SQDG), phosphatidylglycerol (PG), and phosphatidylcholine (PC) by examining spectra and $[M-H]^-$ values were unsuccessful.

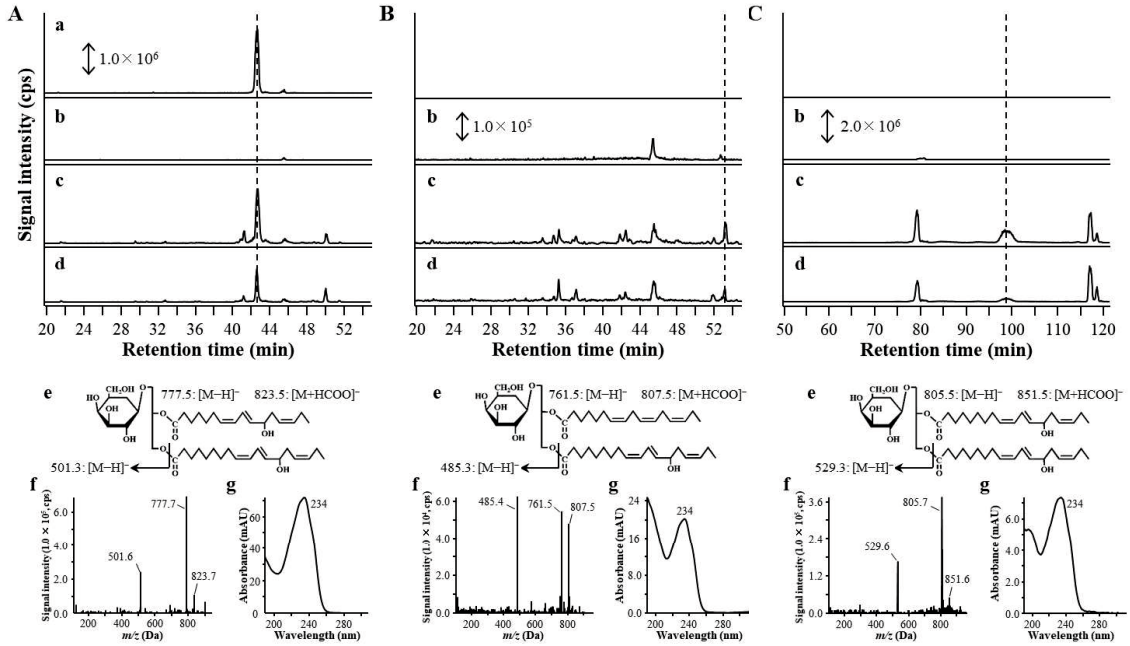

Fig. 21. Detection of MGDG-O(O)Hs in disrupted leaf tissues of Arabidopsis (Col-0). Selected ion chromatograms with *m/z* = 777.5 ± 0.5 corresponding to $[M-H]^-$ of MGDG-13-HOT/11-HHT (A), with 761.5 ± 0.5 corresponding to $[M-H]^-$ of MGDG-13-HOT/C16:3 (B), and with 805.5 ± 0.5 corresponding to $[M-H]^-$ of MGDG-bis-13-HOT (C) are shown. For each panel, a representative chromatogram of a standard molecule of MGDG-13-HOT/11-HHT prepared from MGDG-C18:3/C16:3 with soybean seed LOX-1 (a) (only with A), extract from intact leaves (b), extract from leaves disrupted without BAPTA (c), and extract from leaves disrupted with BAPTA (d) are shown. The chemical structures (e), MS/MS profiles (f) and absorption spectra (g) of the peaks depicted with dotted lines are also shown.

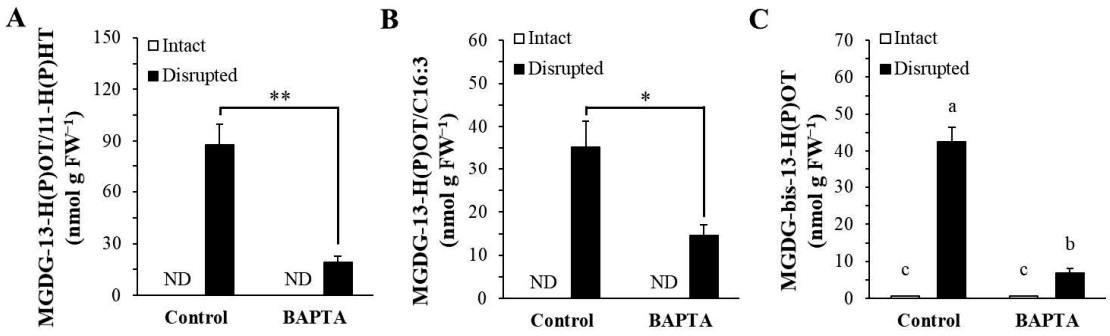

Fig. 22. Amount of MGDG-O(O)Hs in Arabidopsis leaves (Col-0). Mean values ± SEM (error bars) of MGDG-13-H(P)OT/11-H(P)HT (A), MGDG-13-H(P)OT/C16:3 (B), and MGDG-bis-13-H(P)OT (C) are shown (n = 4, biological replicates). Asterisks in panels A and B show significant differences (Student's t-test, *; $P < 0.05$, **; $P < 0.01$). Different letters in panel C show significant differences (two-way ANOVA, Tukey's test, $P < 0.01$).

Effect of BAPTA or EGTA on GLV-burst

While intact Arabidopsis leaves hardly form GLVs, disruption of the leaves results in GLV-burst (described in Chapter 1, Fig. 18) [22]. Some animal LOXs, which involved in the synthesis of leukotrienes, were reported that Ca^{2+} is required for its activation [41,42]. In compared with these crystal structures with modeled Arabidopsis LOX2, I found that candidate amino acid residues (PLAT domain-like structure) in N-terminal (Fig. 23). In order to assess the effect of Ca^{2+} on GLVs formation in Arabidopsis, I used BAPTA and EGTA, Ca^{2+}-specific chelators [54,55]. Addition of BAPTA to the buffer used for disruption significantly suppressed the formation of (*Z*)-3-hexenal, (*E*)-2-hexenal, and 1-penten-3-ol, but not that of (*Z*)-3-hexen-1-ol and *n*-pentan-1-ol (Fig. 24A). Disruption with EGTA also resulted in suppression of GLV-burst in almost a similar manner as that after addition of BAPTA, except for *n*-pentan-1-ol. The formation of *n*-pentan-1-ol slightly but significantly increased in the presence of EGTA (Fig. 24B).

Next, I disrupted Arabidopsis leaves with a buffer containing BAPTA or EGTA supplemented with varying concentrations of Ca^{2+}. The concentrations of free Ca^{2+} ($[Ca^{2+}]_{free}$) in the presence of BAPTA or EGTA were estimated using the dissociation constants of BAPTA or EGTA against Ca^{2+} [54] at pH 6.3 with MaxChelator (http://maxchelator.stanford.edu). The contribution of free Ca^{2+} derived from vacuoles (0.2–5 mM) of Arabidopsis cells, which are the most critical store of free Ca^{2+} [56], was taken into consideration during calculations. In the absence of BAPTA, 338 nmol g FW^{-1} of (*Z*)-3-hexenal was formed, while the addition of BAPTA significantly suppressed its formation (Fig. 25A). A significant suppression was observed even after the addition of $CaCl_2$ to the buffer containing BAPTA to 0.5 mM, where the concentration of $[Ca^{2+}]_{free}$ was estimated to be 0.526–0.834 μM. The suppression was insignificant when $[Ca^{2+}]_{free}$ reached a concentration of 1.50–3.30 μM, and the amount of (*Z*)-3-hexenal formed at the concentration of 1.44–1.54 mM of $[Ca^{2+}]_{free}$ was significantly higher than that found in buffer alone. Increasing the concentration of $[Ca^{2+}]_{free}$ by adding $CaCl_2$ to the buffer containing EGTA yielded almost a similar result even though the amount of $[Ca^{2+}]_{free}$ that eliminated the suppression was higher (82.5–153 μM) than that observed with BAPTA (1.5–3.3 μM) (Fig. 25B). The highest concentration of $CaCl_2$ (2.5 mM; corresponding to 1.44–1.54 mM of $[Ca^{2+}]_{free}$) led to a significant improvement in (*Z*)-3-hexenal formation with EGTA as observed with BAPTA.

When 1 mM of $MgCl_2$ was added to the buffer supplemented with BAPTA, no significant difference in the amount of (*Z*)-3-hexenal formed was observed even though the concentration of $[Mg^{2+}]_{free}$ was estimated to be higher than 1 mM (Fig. 26). Since BAPTA hardly chelates Mg^{2+} in physiological concentration [57], suppression of GLVs formation is caused by chelating Ca^{2+} to inhibit LOX2 activation.

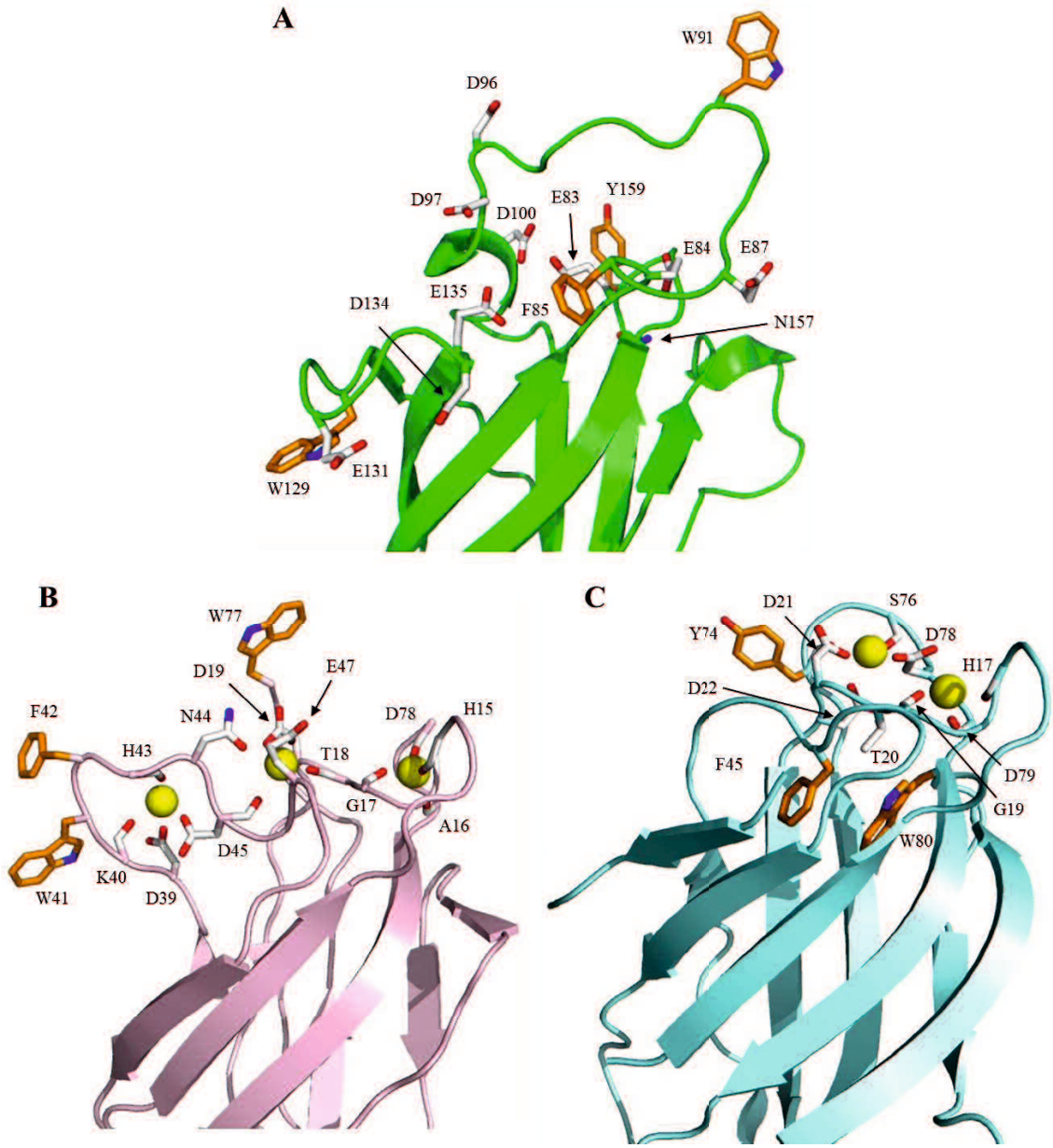

Fig. 23. Model structure of the loop in the PLAT domain of AtLOX2 (A) with the reported structure of coral 8*R*-LOX (B) and human 5-LOX (C). Structure of AtLOX2 excluding predicted chloroplast transit peptide (56 amino acid residues in N-terminal) was modeled based on soybean seed LOX-1 (3PZW) with SWISS-MODEL. Amino acid residues that could have similar roles as observed in coral 8*R*-LOX (2FNQ) [53] and human 5-LOX (3O8Y) [42] is illustrated. Calcium ions are shown with yellow spheres in (B and C).

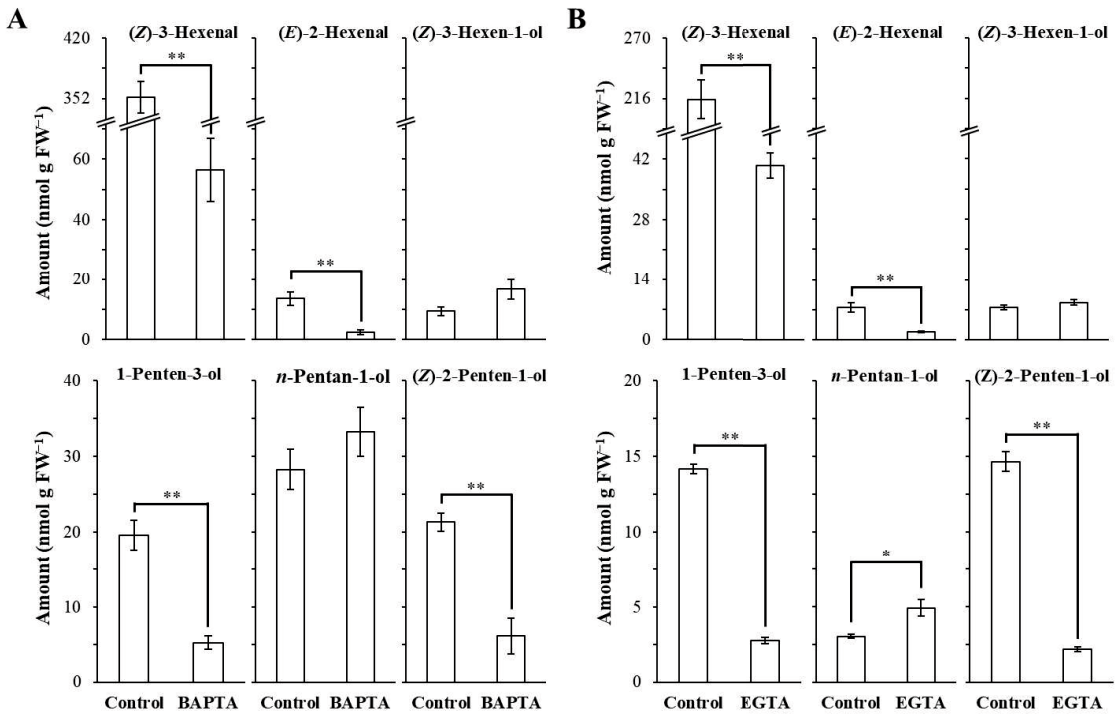

Fig. 24. Effect of addition of BAPTA (A) or EGTA (B) on the amount of volatile compounds formed after complete disruption of Arabidopsis leaves (Ws-1). Mean values ± SEM (error bars) are shown (n = 4, biological replicates). Asterisks show significant difference (Student's t-test, *; $P < 0.05$, **; $P < 0.01$).

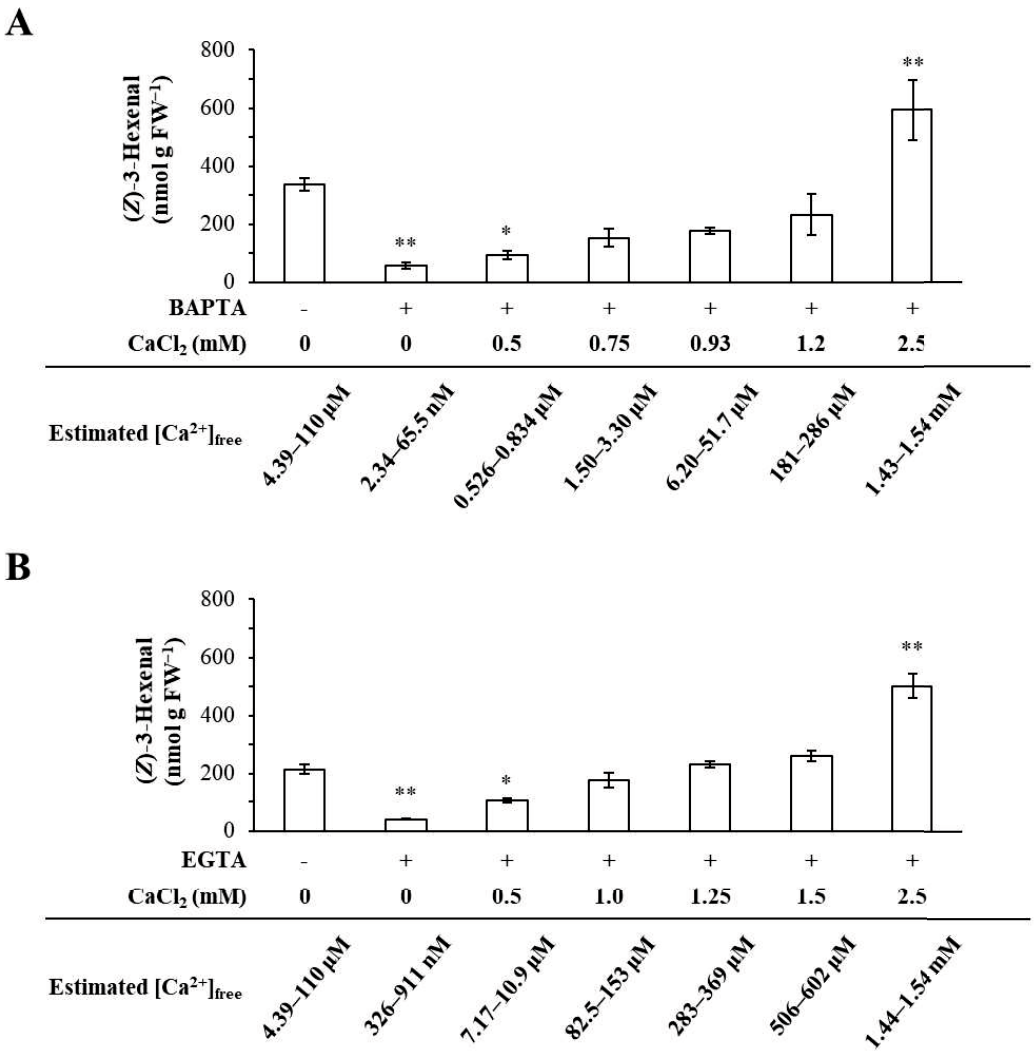

Fig. 25. Effect of $CaCl_2$-supplementation on the suppression of (*Z*)-3-hexenal formation caused by BAPTA (A) and EGTA (B). Arabidopsis leaves (Ws-1) were disrupted in the presence of BAPTA (A) or EGTA (B) supplemented with 0–2.5 mM $CaCl_2$. Estimated concentrations of free Ca^{2+} are shown below each graph. Mean values ± SE are shown (n = 4, biological replicates). Asterisks show significant differences in the amounts of (*Z*)-3-hexenal found without BAPTA or EGTA (one-way ANOVA, Dunnett's test, *; $P < 0.05$, **; $P < 0.01$).

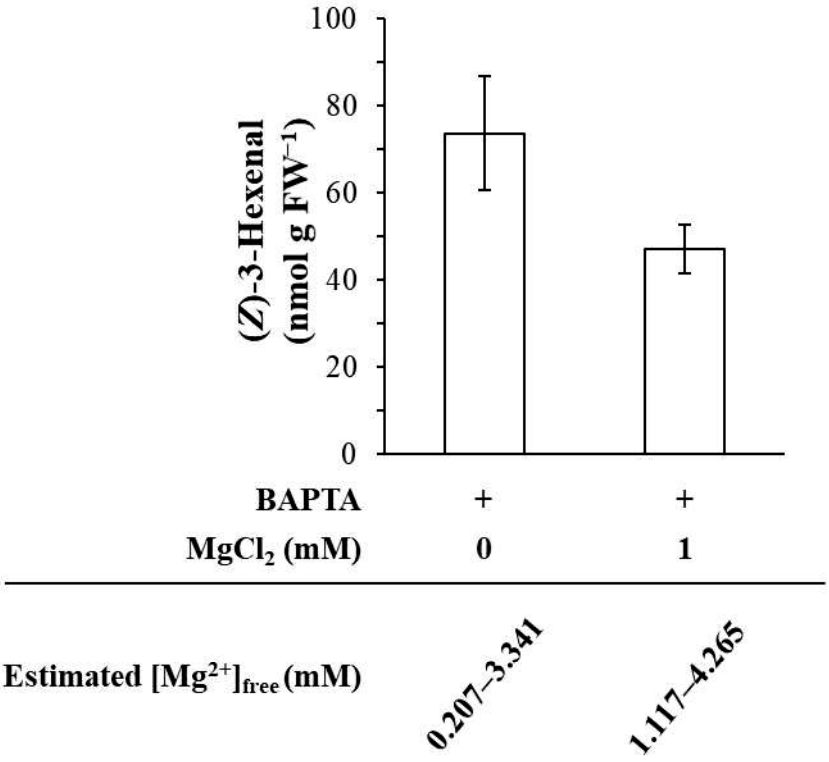

Fig. 26. $MgCl_2$ addition does not relieve the suppression of (*Z*)-3-hexenal formation caused by BAPTA. (*Z*)-3-Hexenal was extracted from completely disrupted Arabidopsis leaves (Ws-1) in the presence of BAPTA supplemented with/without 1 mM $MgCl_2$. Mean values ± SEM (error bars) are shown (n = 4, biological replicates). Estimated $[Mg^{2+}]_{free}$ is shown below the graph. No significant differences were found (Student's t-test, P = 0.11).

Effect of BAPTA on HPL and lipase activity

Addition of BAPTA during the complete disruption of Arabidopsis leaves significantly suppressed the formation of MGDG-OOHs (Fig. 22). The amount of MGDG-OOHs in the presence of BAPTA was 68.6 nmol g FW^{-1}, which was almost equivalent to the amount of (*Z*)-3-hexenal found in disrupted Arabidopsis Ws-1 leaves in the presence of BAPTA (56.3 nmol g FW^{-1}, Fig. 24A). It was assumed that the suppression of GLV-burst by BAPTA was mostly attributable to the effect of BAPTA on AtLOX2 activity. I examined the effect of BAPTA on HPL activity in *lox2-1* mutant with 13-HPOT as a substrate (described in Chapter 1, Fig. 11). Analysis was carried out by using GC-MS. I observed that BAPTA had a minimal effect on HPL activity (Fig. 27), which justified our assumption.

A lipase activity was also investigated. In GLVs biosynthetic pathway, it had been assumed that a lipase was a rate-limiting factor to release free fatty acid as a substrate for LOX. Previously, we found that lipase-independent pathway is accountable for at least part of GLVs formation (more than half of GLVs) [27]; however, it is not impossible to exclude involvement of a lipase activity in GLV-burst. Most animal lipases known to be activated after association with Ca^{2+} [58]. Therefore, BAPTA could affect on GLVs formation through affecting lipase activity. The amounts of free fatty acids in completely disrupted Arabidopsis (*lox2-1*/Ws-1) were analyzed with GC-MS after methyl esterification with diazomethane (Fig. 27). Unexpectedly, a substantial amount of free fatty acids were accumulated even in intact tissues. Among them, linoleic acid (LA) and α-linolenic acid (LNA) could be precursors for GLVs. The amount LA was less than 10 nmol g FW^{-1}. LNA is most abundant free fatty acid detected in this study, and its amount was 79.0 and 57.3 nmol g FW^{-1} in intact leaves and leaf-homogenate incubated for 3 min after disruption, respectively. In the presence of BAPTA, the amount of LNA was significantly decreased to 9.31 nmol g FW^{-1}.

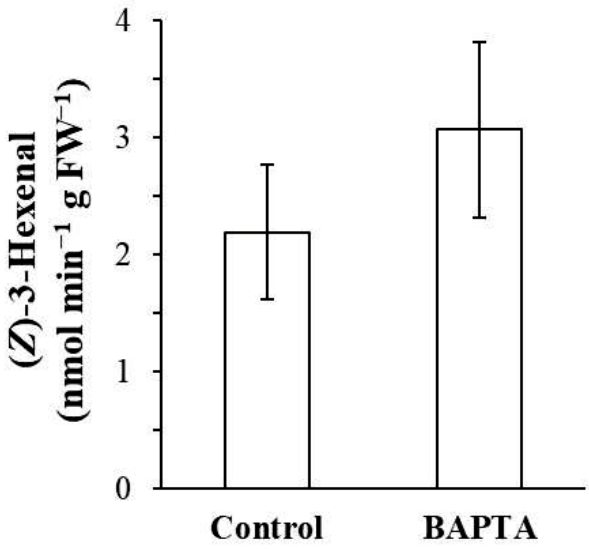

Fig. 27. Effect of BAPTA on HPL activity. Arabidopsis *lox2-1*/Ws-1 mutant was disrupted in the absence or presence of BAPTA, and HPL activity with 13-HPOT was determined. Mean values ± SEM (error bars) are shown (n = 4, biological replicates). No significant differences were found (Student's t-test, P = 0.39).

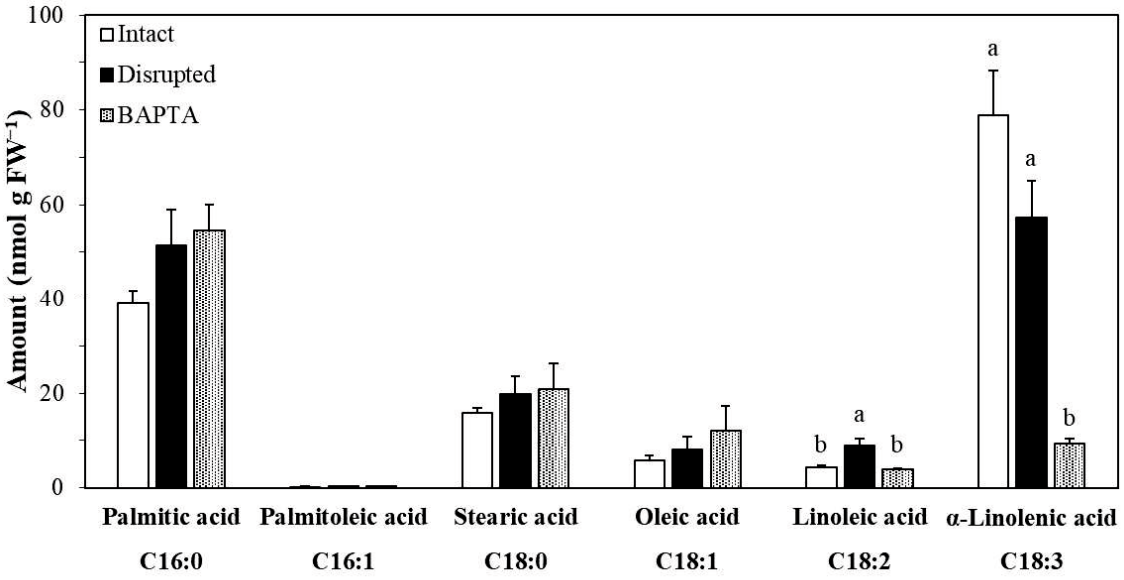

Fig. 28. A lipase activity in Arabidopsis leaves. Free fatty acids were extracted from intact or completely disrupted Arabidopsis (*lox2-1*/Ws-1), methyl-esterified with diazomethane, and analyzed with GC-MS. Mean values ± SEM (error bars) are shown (n = 4, biological replicates). Different letters show significant differences (one-way ANOVA, Tukey's test, $P < 0.01$).

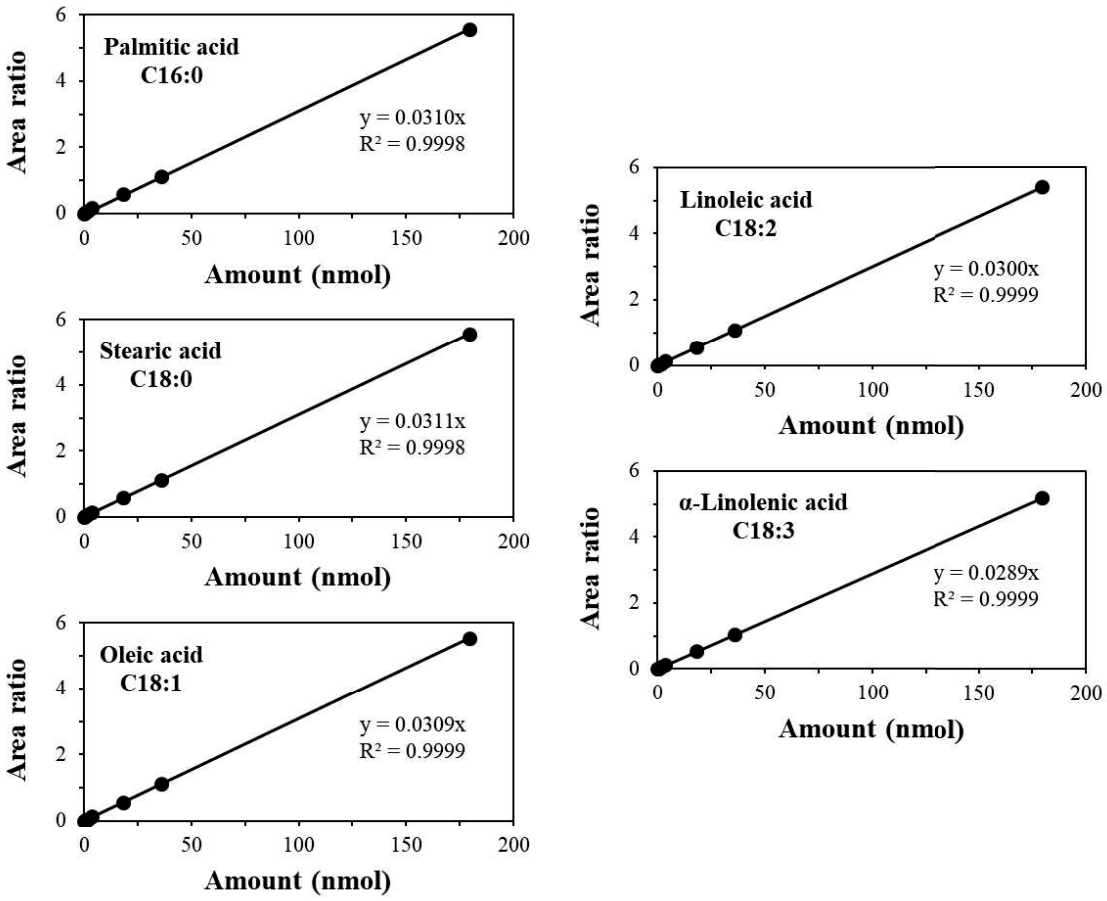

Fig. 29. Calibration curves used for quantification of free fatty acids. The peak areas of total ion chromatogram (TIC) were used for construction of calibration curves.

Effect of BAPTA on GLV-burst in plants

It was suggested that Arabidopsis LOX2 is activated by Ca^{2+}. GLVs are widely conserved oxylipins in almost all terrestrial plants. GLV-burst have been observed empirically in these plants. When I analyze GLVs formation in other plants, all plants except tobacco showed GLV-burst (Fig. 30). Surprisingly, tobacco did not show GLV-burst. Intact tobacco leaves contained relatively high amount of GLVs (1.2 μmol g FW^{-1}), and it accounts for 1.2 mM in its leaf tissues. This is an only exception, and with the other plants intact tissues had low GLV levels and the amounts increased rapidly after disruption of their tissues (Fig. 7).

Our previous study showed that some plants also form a part of GLVs through lipase-independent pathway [27]. Therefore, it was expected that GLV-burst would be controlled by lipoxygenase activity as found with Arabidopsis leaves. When I constructed model structure of tomato LOXC and tobacco LOX2, which were reported to contribute GLVs formation [7,8], amino acid residues, which could interact with Ca^{2+}, were found at almost similar positions as found with Arabidopsis LOX2 (Fig. 31). However, GLV-burst in these plants were hardly affected by addition of BAPTA at 1 mM. GLV-burst was suppressed only with high concentration of BAPTA (10 mM) in clover and soybean (Fig. 32). Unexpectedly, maize showed significant increase of GLVs formation in the presence of 10 mM BAPTA.

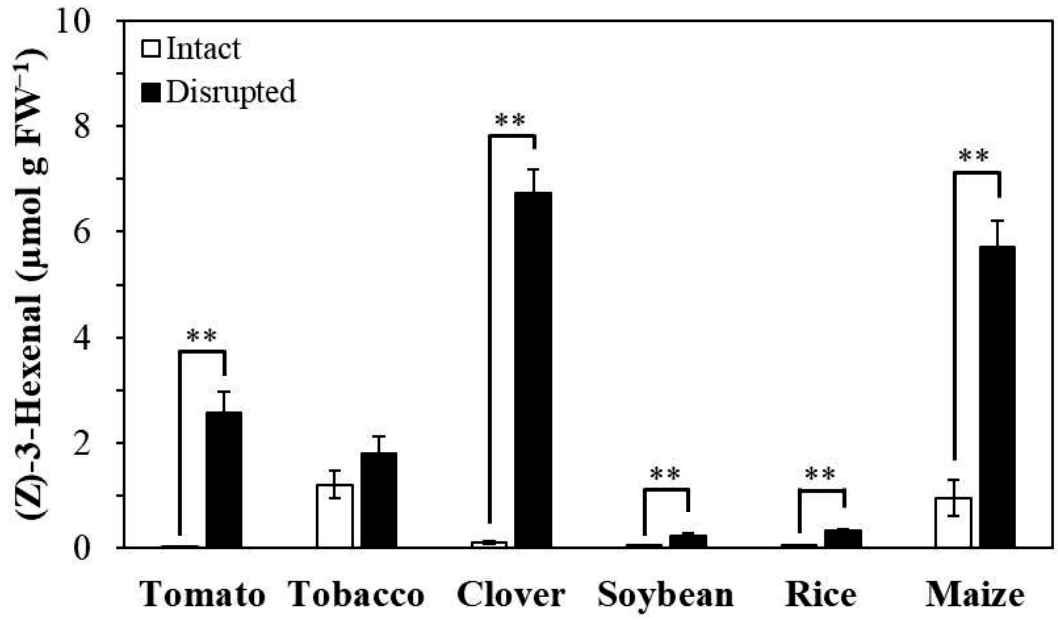

Fig. 30. GLV-burst in several plant species. Mean values ± SEM (error bars) are shown (n = 4, biological replicates). Asterisks show significant difference (Student's t-test, **; $P < 0.01$).

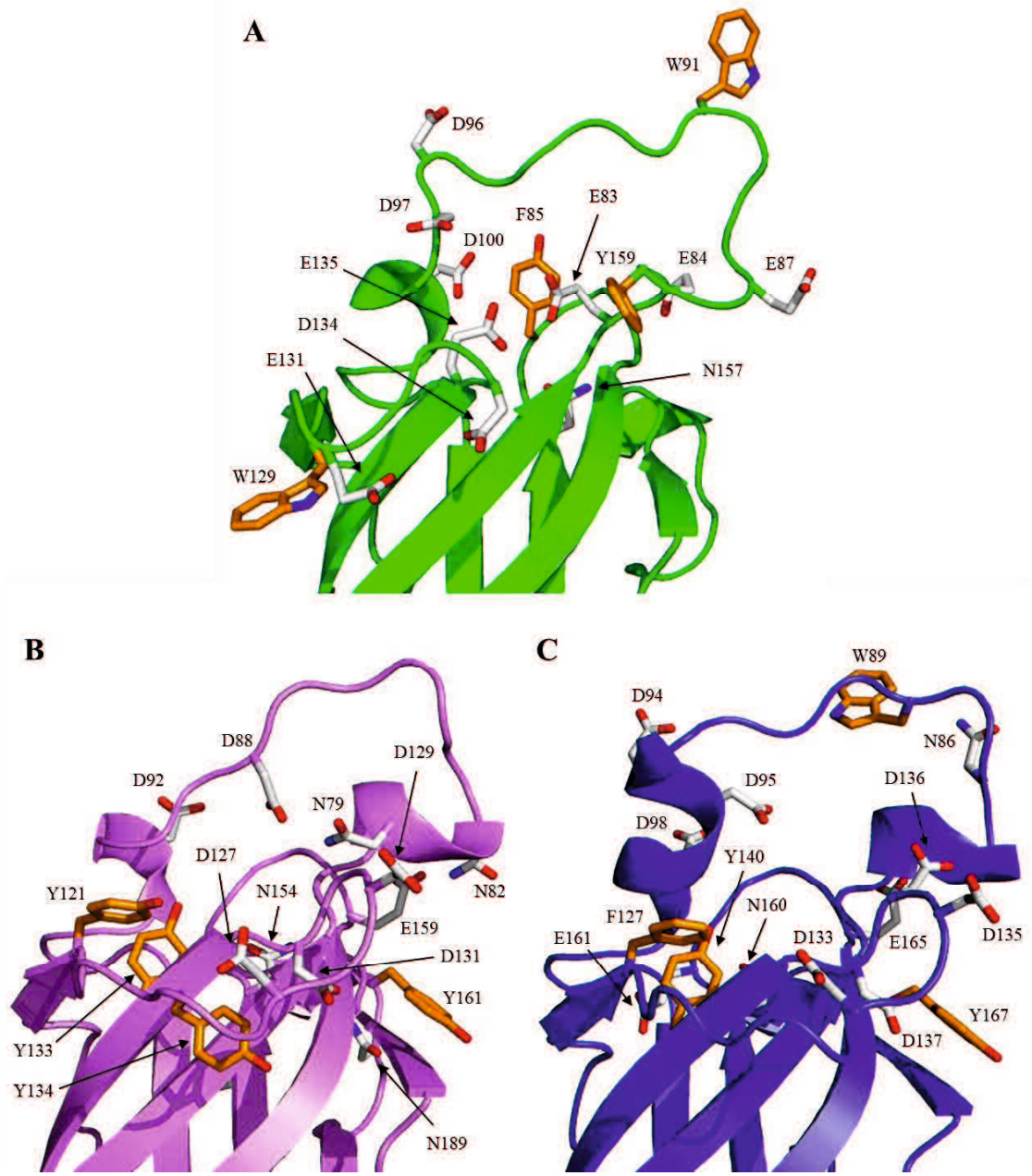

Fig. 31. Model structure of the loop in the PLAT domain of Arabidopsis LOX2 (A), Tomato LOXC (B), and tobacco LOX2 (C). They were modeled based on soybean seed LOX-1 (3PZW) with SWISS-MODEL.

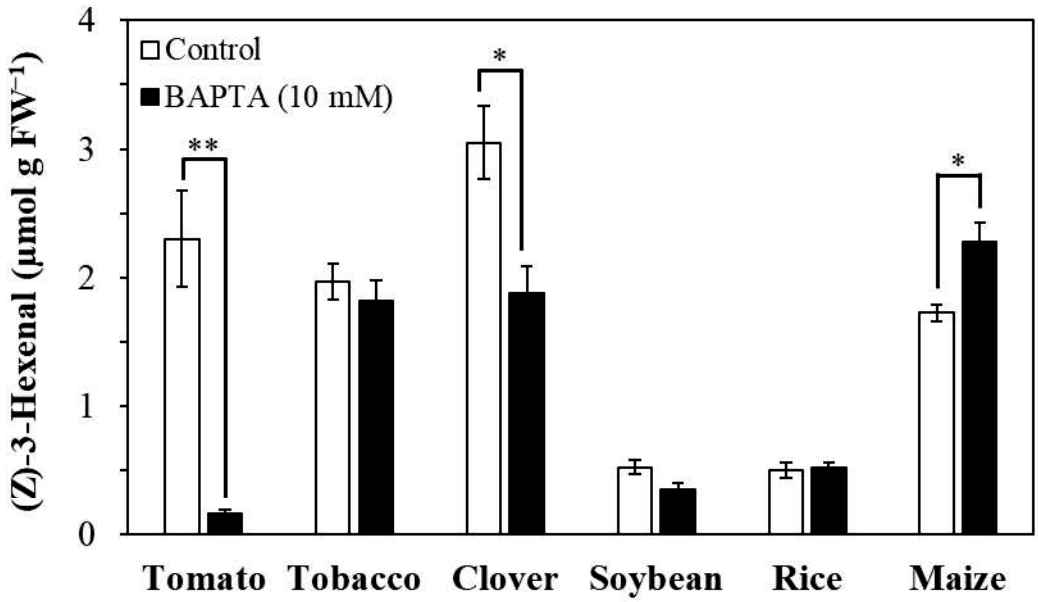

Fig. 32. Effect of BAPTA on GLV-burst in several plant species. Plant leaves were disrupted in the absence or presence of 10 mM BAPTA. Mean values ± SEM (error bars) are shown (n = 4, biological replicates). Asterisks show significant difference (Student's t-test, *; $P < 0.05$, **; $P < 0.01$).

Discussion

GLV-burst, the prompt formation of GLVs following leaf tissue disruption, is observed in most of the terrestrial plant species [4,22,38,39]. However, the specific mechanism of GLV-burst has not been fully understood. In the present study, we observed that BAPTA and EGTA suppressed tissue disruption-triggered GLV-burst in Arabidopsis leaves. The suppression of GLV-burst was relieved by supplementation with Ca^{2+} but not with Mg^{2+} (Figs. 25 and 26). The results implied that Ca^{2+} was largely responsible for the GLV-burst in Arabidopsis leaves. The suppression became insignificant when $[Ca^{2+}]_{free}$ reached a concentration of 1.50–3.30 μM with BAPTA or of 82.5–153 μM with EGTA (Fig. 25). In both cases, the amount of $[Ca^{2+}]_{free}$ required to trigger GLV-burst is almost similar to the amount found in chloroplast stroma of stimulated plant cells [47,59]. However, we are still unable to explain the differences in $[Ca^{2+}]_{free}$ required to relieve the suppression by BAPTA or EGTA. Accurate estimation of $[Ca^{2+}]_{free}$ in the homogenate should be carried out. Moreover, the Ca^{2+} binding speed of BAPTA, which is 150-fold faster than EGTA [55], should be taken into account. The difference in kinetics in chelating Ca^{2+} between BAPTA and EGTA may influence competition for Ca^{2+} between a regulatory factor in the GLV-burst and the chelating reagents.

In Arabidopsis leaves, direct oxygenation of galactolipids by AtLOX2 is the key first committed step in GLV-burst formation (described in Chapter 1, Fig. 2) [27]. In the present study, we observed the rapid formation of MGDG-OOHs following disruption of Arabidopsis leaf tissues (Fig. 21). In addition, the amounts of MGDG-OOHs formed in Col-0 (HPL-deficient ecotype) largely accounted for the (*Z*)-3-hexenal that was formed when the ecotype that had active HPL (such as Ws-1) was used (Figs. 22 and 24). This supports our view that the estimation of the amount of MGDG-OOHs rapidly formed after tissue-disruption is useful in estimating the AtLOX2 activity *ex vivo* that is responsible for GLV-burst. This is the first report directly demonstrating the involvement of MGDG-OOH formation in GLV-burst in Arabidopsis. DGDG-OOHs and OOHs of the other major polar lipids, such as SQDG, PC, or PG were not detected. Especially, the amount of DGDG-bis-C18:3 reaches 43% of MGDG-C18:3/C16:3 or 129% of MGDG-bis-C18:3 [60,61]. Such evidence indicates that AtLOX2 prefers MGDGs as substrates for the formation of corresponding MGDG-OOHs in disrupted leaf tissues where GLV-burst forms.

It has been believed that lipase is a key step of release of free fatty acids from lipids to initiate GLVs formation. When I examined a lipase activity on *lox2-1* mutant, tissue-disruption did not affect on release of LNA (Fig. 28). LA formation was significantly increased after disruption, but its amount is too small (<10 nmol g FW^{-1}). It indicates that almost all GLVs were formed through lipase-independent pathway, because LNA and LA were not accumulated in disrupted *lox2-1* mutant Arabidopsis. This result supports the evidence that MGDG-OOH formation contributes GLV-burst in Arabidopsis. Since BAPTA also suppressed the formation of LNA, the activity of lipase was suppressed by BAPTA. LNA formation was also suppressed in *lox2-1* mutant in the presence of BAPTA, it suggests that LOXs other than LOX2 may consume LNA.

The addition of BAPTA during disruption of Arabidopsis leaves significantly suppressed the formation of MGDG-OOHs (Fig. 22). The degree of suppression of MGDG-OOHs formation was highly correlated with that of (*Z*)-3-hexenal (Fig. 24). Therefore, it was concluded that the suppression of AtLOX2 activity on MGDG by the addition of BAPTA was the primary cause of suppression of GLV-burst in Arabidopsis. Considering these results, we propose that AtLOX2 stays inactive in the chloroplast stroma of intact Arabidopsis leaf cells and that AtLOX2 is activated by Ca^{2+} derived from other compartments, most probably from vacuoles, apoplasts, or from thylakoid lumen [47], upon the disruption of leaf tissues. The basal concentration of $[Ca^{2+}]_{free}$ in chloroplast stroma in unstressed leaves ranges from 0.1–0.2 μM [48,56], which is substantially lower than that required to completely relieve the suppression of GLV-burst caused by BAPTA or EGTA. Stimulation of Arabidopsis cells with several environmental stimuli, such as H_2O_2, salt stress, osmotic stress, cold shock, or elicitor, led to a rapid increase in the concentration of $[Ca^{2+}]_{free}$ (0.39–0.92 μM) in stroma [59]. Even though the concentration of $[Ca^{2+}]_{free}$ reported with stimulated Arabidopsis cells is still a little lower than the level observed to be critical for relieving the suppression of GLV-burst caused by BAPTA or EGTA, such tight regulation of $[Ca^{2+}]_{free}$ in stroma might be one of the factors exploited by the inducible defense system present in chloroplast stroma. It is likely that such tight regulation would be disordered vigorously by tissue disruption, which would cause increase in the concentration of $[Ca^{2+}]_{free}$ in the bulk solution surrounding AtLOX2, and subsequently activate AtLOX2 to initiate its activity on MGDG.

Some LOXs in both animal and plant tissues are translocated to biological membranes upon cell stimulation in a Ca^{2+}-dependent manner [62]. In stimulated human cells, Ca^{2+}-dependent translocation of 5-LOX to nuclear membranes takes place, which triggers the formation of bioactive lipid mediators including leukotrienes [43]. Coral (*Gersemia fruticosa*) 11*R*-LOX also requires Ca^{2+} to be translocated to membranes with appropriate compositions of phospholipid species [63]. Crystal structure analyses of 8*R*-LOX [53], 11*R*-LOX [64], and 15-LOX-2 [65] revealed that association with Ca^{2+} seems to alter the configuration of loops that emerge from the edge of the β-barrel in PLAT domains, which expose hydrophobic amino acid residues, such as Trp or Phe (Fig. 23). This might also be the case with some plant LOXs. Soybean seed LOX-1 undergoes a Ca^{2+}-regulated membrane binding that is under the control of its PLAT domain [44,66]. Association of maize LOX-1 with cell membranes is also facilitated by the addition of Ca^{2+}, and N-terminal PLAT domain is critical for the association [45]. Modeling the structure of AtLOX2 based on soybean seed LOX-1 structure enabled us to illustrate Glu and Asp residues that were located in the loops similar to those observed in coral 8*R*-LOX and human 5-LOX (Fig. 23). Based on the above factors, it is suggested that AtLOX2 is present in its latent, soluble form in chloroplast stroma in unstimulated cells but the increase in the concentration of $[Ca^{2+}]_{free}$ in the bulk solution surrounding AtLOX2 facilitates binding of Ca^{2+} with acidic amino acid residues residing in or near the loops in PLAT domain, which subsequently alters the configuration of the loop to provide hydrophobicity enough to associate with the membrane. This sequence of events triggers GLV-burst in Arabidopsis leaves. In order to confirm this, detailed *in vitro* investigations with purified AtLOX2 are underway.

In the plant species, such as tomato, tobacco, clover, soybean, rice, or maize, all plants except tobacco showed clear GLV-burst as found with Arabidopsis (Fig. 30). Tobacco leaves contained substantial level of (*Z*)-3-hexenal in intact tissues and complete disruption of leaves caused essentially no effect on the amounts. It is reported that tobacco forms GLVs depending on circadian-imposed physiological constraints [67], which suggests that tobacco might have a mechanism to regulate LOX activity even in intact cells. A study revealed that high concentration of (*Z*)-3-hexenal is toxic for Arabidopsis (>40 μM as vapor) [23,68], therefore, tobacco leaf tissues should have a countermeasure to avoid the toxicity. A specific deposition of the chemical into a specific structure, such as trichomes, might be one of the ways to avoid autointoxication. Even though maize also contained high amount of (*Z*)-3-hexenal in intact tissues (956 μM), this high amount might be caused by unexpected wounding during sample preparation because maize leaf is long and hard to handle. In the structure model of tomato LOXC and tobacco LOX2, Asp and Glu rich region was found at the similar positions found with Arabidopsis LOX2 (Fig. 31). However, GLV-burst in tomato and tobacco leaves were not affected in the presence of 1 mM BAPTA and 10 mM BAPTA was needed to significant suppression of GLV-burst in tomato and clover. Further experiment using purified LOX with Ca^{2+} *in vitro* is required.

Human 5-LOX is well characterized as a post-translationally modified enzyme. Other than Ca^{2+}-activation, substantial roles of 5-LOX activating protein (FLAP) and phosphorylation in regulation of its activity were well studied [69,70]. Any homologs of FLAP in plants are not found with protein BLAST search in NCBI (https://blast.ncbi.nlm.nih.gov/Blast.cgi). It has been reported that phosphorylation of 5-LOX modulates activity [70–72], but the mechanism of phosphorylation-dependent activation is still unknown. Several Ser and Tyr are characterized as the phosphorylation site in 5-LOX [70], and Arabidopsis LOX2 model also suggests Ser and Tyr in similar region (Fig. 33); however, further studies are essential to get insight about the effect of phosphorylation of plant LOXs on their activity. Even though I show that Ca^{2+} is critical for GLV-burst in Arabidopsis LOX2, there must be the other mechanisms to regulate GLV-burst as the effect of BAPTA on GLV-burst in other plant species somewhat varies. Mechanisms to regulate LOX activity, such as FLAP-like protein or phosphorylation, must be taken into account.

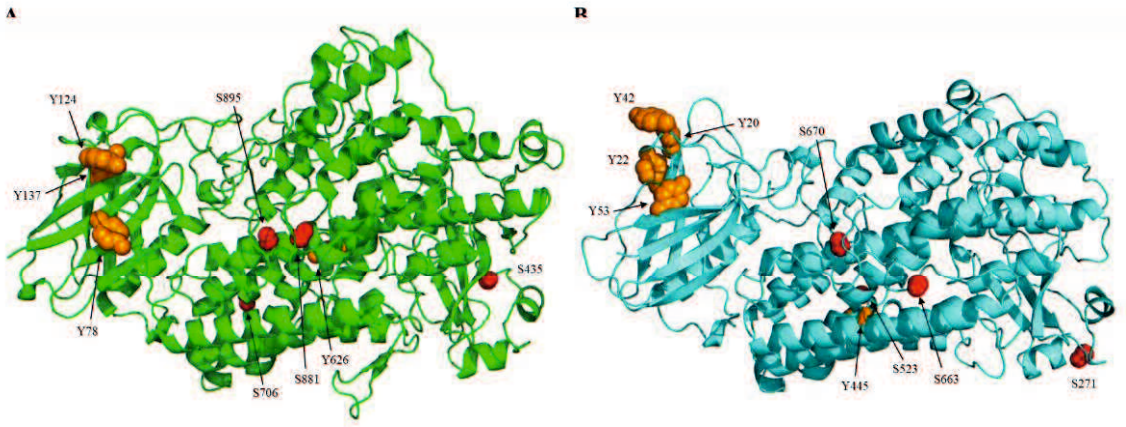

Fig. 33. Phosphorylation site of model structure of Arabidopsis LOX2 (A) with the reported structure of human 5-LOX (B). Amino acid residues that could be phosphorylated as observed in human 5-LOX are illustrated. Ser and Tyr were shown with red spheres and pink spheres, respectively.

SUMMARY

In this thesis, I addressed the mechanism of plant LOX activation that involved in GLV-burst in Arabidopsis. Arabidopsis LOX2 was identified as an essential LOX to form GLVs and five carbon volatile compounds by using a complete set of knockout mutant of each *LOX* gene in Chapter 1. A LOX involved in GLVs and/or JA formation has been identified in several plant species, and it has distinct role to form GLVs or JA. However, it was already known that Arabidopsis LOX2 is also essential to generate the relatively high levels of JA after wounding. Taken together with my findings, Arabidopsis LOX2 is an unique enzyme, which exerts bifunctional involvement to form the two types of oxylipins.

In Chapter 2, I clarified that Ca^{2+} is the factor to activate Arabidopsis LOX2 to initiate oxidization of MGDG to form corresponding OOHs, which directly contributes GLV-burst. 3D-modeling revealed that the structure of Arabidopsis LOX2 has amino acid residues, which could contribute to Ca^{2+} binding and membrane association at the similar positions with those observed in animal LOXs that are reported as Ca^{2+}-dependent enzymes. Tomato LOXC and Tobacco LOX2 are also involved in GLVs formation, with similar amino acid residues in their 3D-model. However, GLV formation in tomato and tobacco were not affected by BAPTA. It is possible that FLAP-like protein or phosphorylation, which activates animal LOXs, regulates LOX activity in these plants. LOX is the key enzyme to defense against various enemies through facilitating oxylipin-burst. MGDG is substrate of LOX and also major component of thylakoid membrane (about 50% of thylakoid membrane lipid), which is essential to develop plant itself. Therefore, oxylipin burst should not occur in intact tissues while it should be promptly activated upon damage on the tissues caused by enemies. The tight regulation is indispensible to support inducible defense against biotic attack.

REFERENCES

[1] Mosblech, A., Feussner, I., and Heilmann, I. Oxylipins: structurally diverse metabolites from fatty acid oxidation. *Plant Physiol. Biochem*. **47**, 511–517 (2009).

[2] Pohl, C.H., and Kock, J.L.F. Oxidized fatty acids as inter-kingdom signaling molecules. *Molecules*. **19**, 1273–1285 (2014).

[3] Matsui, K. Green leaf volatiles: hydroperoxide lyase pathway of oxylipin metabolism. *Curr. Opin. Plant Biol*. **9**, 274–280 (2006).

[4] Scala, A., Allmann S., Mirabella, R., Haring, M.A., and Schuurink, R.C. Green leaf volatiles: a plant's multifunctional weapon against herbivores and pathogens. *Int. J. Mol. Sci*. **14**, 17781–17811 (2013).

[5] Wasternack, C. and Hause, B. Jasmonates: biosynthesis, perception, signal transduction and action in plant stress response, growth and development. An update to the 2007 review in *Annals of Botany*. *Ann. Bot*. **111**, 1021–1058 (2013).

[6] Mwenda, C.M., Matsuki, A., Nishimura, K., Koeduka, T., and Matsui, K. Spatial expression of the Arabidopsis hydroperoxide lyase gene is controlled differently from that of the allene oxide synthase gene. *J. Plant Interact*. **10**, 1–10 (2015).

[7] Allman, S., Halitschke, R., Schuurink, R.C., and Baldwin, I.T. Oxylipin channeling in *Nicotiana attenuata*: lipoxygenase 2 supplies substrates for green leaf volatile production. *Plant Cell Environ*. **33**, 2028–2040 (2010).

[8] Shen, J., Tieman, D., Jones, J.B., Taylor, M.G., Schmelz, E., Huffaker, A., Bies, D., Chen, K., Klee, H.J. (2014) A 13-lipoxygenase, TomloxC, is essential for synthesis of C5 flavor volatiles in tomato. *J. Exp. Bot*. **65**, 419–428 (2014).

[9] León, J., Royo, J., Vancanneyt, G., Sanz, C., Silkowski, H., Griffiths, G., Sánchez-Serrano, J.J. Lipoxygenase H1 gene silencing reveals a specific role in supplying fatty acid hydroperoxides for aliphatic aldehyde production. *J. Biol. Chem*. **277**, 416–423 (2002).

[10] Christensen, A.S., Nemchenko, A., Borrego, E., Murray, I., Sobhy, I.S., Bosak, L., DeBlasio, S., Erb, M., Robert, C.A.M., Vaughn, K.A., Herrfurth, C., Tumlinson, J., Feussner, I., Jackson, D., Turlings, T.C.J., Engelberth, J., Nansen, C., Meeley, R., Kolomiets, M.V. The maize lipoxygenase, *ZmLOX10*, mediates green leaf volatile, jasmonate and herbivore-induced plant volatile production for defense against insect attack. *Plant J*. **74**, 59–73 (2013).

[11] Zhou, G., Qi, J., Ren, N., Cheng, J., Erb, M., Mao, B., and Lou, Y. Silencing *OsHI-LOX* makes rice more susceptible to chewing herbivore, but enhances resistance to a phloem feeder. *Plant J*. **60**, 638–648 (2009).

[12] Halitschke, R. and Baldwin, I.T. Antisense LOX expression increases herbivore performance by decreasing defense responses and inhibiting growth-related transcriptional reorganization in *Nicotiana attenuata*. *Plant J*. **36**, 794–807 (2003).

[13] Yan, L., Zhai, Q., Wei, J., Li, S., Wang, B., Huang, T., Du, M., Le, S., Li, C.B., Li, C. Role of tomato lipoxygenase D in wound-induced jasmonate biosynthesis and plant immunity to insect

herbivores. *PLoS ONE*. **9**, e1003964 (2013).

[14] Wang, R., Shen, W., Liu, L., Jiang, L., Liu, Y., Su, N., Wan, J. A novel lipoxygenase gene from developing rice seeds confers dual position specificity and responds to wounding and insect attack. *Plant Mol. Biol*. **66**, 401–414 (2008).

[15] Chauvin, A., Caldelari, D., Wolfender, J.-L., and Farmer, E.E. Four 13-lipoxygenases contributed to rapid jasmonate synthesis in wounded *Arabidopsis thaliana* leaves: a role for lipoxygenase 6 in response to long-distance wound signals. *New Phytol*. **197**, 566–575 (2013).

[16] Bell, E., Creelman, R.A., and Mullet, J.E. A chloroplast lipoxygenase is required for wound-induced jasmonic acid accumulation in *Arabidopsis*. *Proc. Natl. Acad. Sci. USA*. **92**, 8675–8679 (1995).

[17] Caldelari, D., Wang, G., Farmer, E.E., and Dong, X. Arabidopsis *lox3 lox4* double mutants are male sterile and defective in global proliferative arrests. *Plant Mol. Biol*. **75**, 25–33 (2011).

[18] Gasperini, D., Chauvin, A., Acosta, I.F., Kurenda, A., Stolz, S., Chételat, A., Wolfender, J.-L., and Farmer, E.E. Axial and radial oxylipin transport. *Plant Physiol*. **169**, 2244–2254 (2015).

[19] Grebner, W., Stingl, N.E., Oenel, A., Mueller, M.J., and Berger, S**.** Lipoxygenase6-dependent oxylipin synthesis in roots is required for abiotic and biotic stress resistance of Arabidopsis. *Plant Physiol*. **161**, 2159–2170 (2013).

[20] Vellosillo, T., Martínez, M., López, M.A., Vicente, J., Cascón, T., Dolan, L., Hamberg, M., and Castresana, C. Oxylipins produced by the 9-lipoxygenase pathway in *Arabidopsis* regulate lateral root development and defense responses through a specific signaling cascade. *The Plant Cell*. **19**, 831–846 (2007).

[21] Zoeller, M., Stingl, N., Krischke, M., Fekete, A., Waller, F., Berger, S., and Mueller, M.J. Lipid profiling of the Arabidopsis hypersensitive response reveals specific lipid peroxidation and fragmentation processes: biogenesis of pimelic and azelaic acid. *Plant Physiol*. **160**, 365–378 (2012).

[22] D'Auria, J.C., Pichersky, E., Schaub, A., Hansel, A., and Gershenzon, J. Characterization of a BAHD acyltransferase responsible for producing the green leaf volatile (*Z*)-3-hexen-1-yl acetate in *Arabidopsis thaliana*. *Plant J*. **49**, 194–207 (2007).

[23] Matsui, K., Sugimoto, K., Mano, J., Ozawa, R., and Takabayashi, J. Differential metabolisms of green leaf volatiles in injured and intact parts of a wounded leaf meet distinct ecophysiological requirements. *PLoS ONE*. **7**, e36433 (2012).

[24] Maja, M.M., Kasurinen, A., Yli-Pirilä, P., Joutsensaari, J., Klemola, T., Holopainen, T., and Holopainen, J.K. Contrasting responses of silver birch VOC emissions to short- and long-term herbivory. *Tree Physiol*. **34**, 241–252 (2014).

[25] Glauser, G., Dubugnon, L., Mousavi, S.A.R., Rudaz, S., Wolfender, J.-L., and Farmer, E.E. Velocity estimates for signal propagation leading to systemic jasmonic acid accumulation in wounded *Arabidopsis*. *J. Biol. Chem*. **284**, 34506–34513 (2009).

[26] Wittstock, U. and Halkier, B.A. Glucosinolate research in the Arabidopsis era. *Trends Plant Sci*. **7**, 263–270 (2002).

[27] Nakashima, A., von Reuss, S.H., Tasaka, H., Nomura, M., Mochizuki, S., Iijima, Y., Aoki, K., Shibata, D., Boland, W., Takabayashi, J., and Matsui, K. Traumatin- and dinortraumatin-containing galactolipids in *Arabidopsis*: Their formation in tissue-disrupted leaves as counterparts of green leaf volatiles. *J. Biol. Chem*. **288**, 26078–26088 (2013).

[28] Duan, H., Huang, M.-Y., Palacio, K., and Schuler, M.A. Variations in *CYP74B2* (hydroperoxide lyase) gene expression differentially affect hexenal signaling in the Columbia and Landsberg *erecta* ecotypes of Arabidopsis. *Plant Physiol*. **139**, 1529–1544 (2005).

[29] Alonso, J.M., Stepanova, A.N., Leisse, T.J., Kim, C.J., Chen, H., Shinn, P., Stevenson, D.K., Zimmerman, J., Barajas, P., Cheuk, R., Gadrinab, C., Heller, C., Jeske, A., Koesema, E., Meyers, C.C., Parker, H., Prednis, L., Ansari, Y., Choy, N., Deen, H., Geralt, M., Hazari, N., Hom, E., Karnes, M., Mulholland, C., Ndubaku, R., Schmidt, I., Guzman, P., Aguilar-Henonin, L., Schmid, M., Weigal, D., Carter, D.E., Marchand, T., Risseeuw, E., Brogden, D., Zeko, A., Crosby, W.L., Berry, C.C., and Ecker, R. Genome-Wide Insertional Mutagenesis of *Arabidopsis thaliana*. *Science*. **301**, 653–657 (2003).

[30] Edwards, K., Johnstone, C., and Thompson, C. A simple and rapid method for the preparation of plant genomic DNA for PCR analysis. *Nucleic Acids Res*. **19**, 1349 (1991).

[31] Koeduka, T., Kimitsune, Ishizaki., Mwenda, C.M., Hori, K., Sasaki-Sekimoto, Y., Ohta, H., Kohchi, T., and Matsui, K. Biochemical characterization of allene oxide synthases from the liverwort *Marchantia polymorpha* and green microalgae *Klebsormidium flaccidum* provides insight into the evolutionary divergence of the plant CYP74 family. *Planta*. **242**, 1175–1186 (2015).

[32] Mwenda, C.M. and Matsui, K. The importance of lipoxygenase control in the production of green leaf volatiles by lipase-dependent and independent pathways. *Plant Biotechnol*. **31**, 445–452 (2015).

[33] Kourtchenko, O., Andersson, M.X., Hamberg, M., Brunnström, Å, Göbel, C., McPhail, K.L., Gerwick, W.H., Feussner, I., and Ellerström, M. Oxo-phytodienoic acid-containing galactolipids in Arabidopsis: Jasmonate signaling dependence. *Plant Physiol*. **145**, 1658–1669 (2007).

[34] Buseman, C.M., Tamura, P., Sparks, A.A., Baughman, E.J., Maatta, S., Zhao, J., Roth, M.R., Wynn Esch, S., Shah, J., Williams, T.D., and Welti, R. Wounding stimulates the accumulation of glycerolipids containing oxophytodienoic acid and dinor-oxophytodienoic acid in Arabidopsis leaves. *Plant Physiol*. **142**, 28–39 (2006).

[35] Peltier, J.B., Cai, Y., Sun, Q., Zabrouskov, V., Giacomelli, L., Rudella, A., Ytterberg, A.J., Rutschow, H., and van Wijk, K.J. The oligomeric stromal proteome of *Arabidopsis thaliana* chloroplasts. *Mol. Cell. Proteomics*. **5**, 114–133 (2006).

[36] Mashima, R. and Okuyama, T. The role of lipoxygenases in pathophysiology; new insights and future perspective. *Redox Biol*. **6**, 297–310 (2015).

[37] Skaterna, T.D., Kopich, V.M., Kharitonenko, G.I., and Kharchenko, O.V. Lipoxygenase regulation *in vivo* and *in vitro* by lipid compounds. *Biopolym. Cell*. **31**, 161–173 (2015).

[38] Matsui, K. Green leaf volatiles: hydroperoxide lyase pathway of oxylipin metabolism. *Curr. Opin. Plant Biol.* **9** (2006) 274–280.

[39] Ameye, M., Allmann, S., Verwaere, J., Smagghe, G., Haesaert, G., Schuurink, R.C., and Audenaert, K. Green leaf volatile production by plants: a meta-analysis. *New Phytol.* **220**, 666–683 (2018).

[40] Arimura, G.I., Matsui, K., and Takabayashi, J. Chemical and molecular ecology of herbivore-induced plant volatiles; proximatefactors and their ultimate functions. *Plant Cell Physiol.* **50**, 911–923 (2009).

[41] Rådmark, O., Werz, O., Steinhilber, D., and Samuelsson, B. 5-Lipoxygenase, a key enzyme for leukotriene biosynthesis in health and disease. *Biochim. Biophys. Acta*. **1851**, 331–339 (2015).

[42] Kulkarni, S., Das, S., Funk, C.D., Murray, D., and Cho, W. Molecular basis of the specific subcellular localization of the C2-like domain of 5-lipoxygenase. *J. Biol. Chem.* **277**, 13167–13174 (2002).

[43] Hammarberg, T., Provost, P., Persson, B., and Rådmark, O. The N-terminal domain of 5-lipoxygenase binds calcium and mediates calcium stimulation of enzyme activity. *J. Biol. Chem.* **275**, 38787–38793 (2000).

[44] Tatulian, S.A., Steczko, J., and Minor, W. Uncovering a calcium-regulated membrane binding mechanism for soybean lipoxygenase-1. *Biochemistry.* **37**, 15481–15490 (1998).

[45] Cho, K., Han, J., Rakwal, R., and Han, O. Calcium modulates membrane association, positional specificity, and product distribution in dual positional specific maize lipoxygenase-1. *Bioorg. Chem.* **60**, 13–18 (2015).

[46] Conn, S. and Gilliham, M. Comparative physiology of elemental distributions in plants. *Ann. Bot.* **105**, 1081–1102 (2010).

[47] Nomura, H. and Shiina, R. Calcium signaling in plant endosymbiotic organelles: mechanism and role in physiology. *Mol Plant.* **7**, 1094–1104 (2014).

[48] Sai, J. and Johnson, C.H. Dark-stimulated calcium ion fluxes in the chloroplast stroma and cytosol. *Plant Cell.* **14**, 1279–1291 (2002).

[49] Toyota, M., Spencer, D., Sawai-Toyota, S., Jiaqi, W., Zhang, T., Koo, A.J., Howe, G.A., and Gilroy, S. Glutamate triggeres long-distance, calcium-based plant defense signaling. *Science.* **361**, 1112–1115 (2018).

[50] Jud, W., Vanzo, E., Ghirardo, A., Zimmer, I., Sharkey, T.D., Hansel, A., and Schnitzler, J.P. Effects of heat and drought stress on post-illumination bursts of volatile organic compounds in isoprene-emitting and non-emitting poplar. *Plant Cell Environ.* **39**, 1204–1215 (2016).

[51] Nakashima, A., Iijima, Y., Aoki, K., Shibata, D., Sugimoto, K., Takabayashi, J., and Matsui, K. Monogalactosyl diacylglycerol is a substrate for lipoxygenase: its implications for oxylipin formation directly from lipids. *J Plant Interact.* **6**, 93–97 (2011).

[52] Arnold, K., Bordoli, J., Kopp, J., and Schwede, T. The SWISS-MODEL Workspace: A web-based environment for protein structure homology modelling. *Bioinformatics.* **22**, 195–201 (2006).

[53] Oldham, M.L., Brash, A.R., and Newcomer, M.E. Insights from the X-ray crystal structure of coral 8*R*-lipoxygenase: calcium activation via a C2-like domain and a structural basis of product chirality. *J. Biol. Chem.* **280**, 39545–39552 (2005).

[54] Simon, M.H. and Bers, D.M. The effect of temperature and ionic strength on the apparent Ca-affinity of EGTA and the analogous Ca-chelators BAPTA and dibromo-BAPTA. *Biochim. Biophys. Acta.* **925**, 133–143 (1987).

[55] Smith, G.A., Hesketh, R.T., Metcalfe, J.C., Feeney, J., and Morris, P.G. Intracellular calcium measurements by ^{19}F NMR of fluorine-labeled chelators. *Proc. Natl. Acad. Sci. USA.* **80**, 7178–7182 (1983).

[56] Steal, S., Wurzinger, B., Mair, A., Mehlmer, N., Vothknecht, V.C., and Teige, M. Plant organellar calcium signaling: an emerging field. *J. Exp. Bot.* **63**, 1525–1542 (2012).

[57] Tsien, R.Y. New calcium indicators and buffers with High selectivity against magnesium and protons: Design, synthesis, and properties of prototype structures. *Biochemistry.* **19**, 2396–2404 (1980).

[58] Hills, M.J. and Beevers, H. Ca^{2+} stimulated neutral lipase activity in castor bean lipid bodies. *Plant Physiol.* **84,** 272–276 (1987).

[59] Sello, S., Perotto, J., Carraretto, L., Szabó, I., Vothknecht, U.C., and Navazio, L. Dissecting stimulus-specific Ca^{2+} signals in amyloplasts and chloroplasts of *Arabidopsis thaliana* cell suspension cultures. *J. Exp. Bot.* **67**, 3965–3974 (2016).

[60] Djafi, N., Humbert, L., Rainteau, D., Cantrel, C., Zachowski, A., and Ruelland, E. Multiple reaction monitoring mass spectrometry is a powerful tool to study glycerolipid composition in plants with different level of desaturase activity. *Plant Singnal Behav.* **8**, e24118 (2013).

[61] Welti, R., Li, W., Li, M., Sang, Y., Biesiada, H., Zhou, H.E., Rajashekar, C.B., Williams, T.D., and Wang, X. Profiling membrane lipids in plant stress responses: role of phospholipase Dα in freezing-induced lipid changes in *Arabidopsis*. *J. Biol. Chem.* **277**, 31994–32002 (2002).

[62] Nwecomer, M.E. and Brash, A.R. The structural basis for specificity in lipoxygenase catalysis. *Protein Sci.* **24**, 298–309 (2014).

[63] Järving, R., Lõokene, A., Kurg, R., Siimon, L., Järving, I., and Samel, N. Activation of 11*R*-lipoxygenase is fully Ca^{2+}-dependent and controlled by the phospholipid composition of the target membrane. *Biochemistry.* **51**, 3310–3320 (2012).

[64] Eek, P., Järving, R., Järving, I., Gilbert, N.C., Newcomer, M.E., and Samel, N. Structure of a calcium-dependent 11*R*-lipoxygenase suggests a mechanism for Ca^{2+} regulation. *J. Biol. Chem.* **287**, 22377–22386 (2012).

[65] Kobe, M.J., Neau, D.B., Mitchell, C.E., Bartlett, S.G., and Newcomer, M.E. The structure of human 15-lipoxygenase-2 with a substrate mimic. *J. Biol. Chem.* **289**, 8562–8569 (2014).

[66] Maccarrone, M., Salucci, M.L., van Zadelhoff, G., Malatesta, F., Velding, G., Viegenthart, J.F.G., and Finazzi-Agró, A. Tryptic digestion of soybean lipoxygenase-1 generates a 60 kDa fragment with improved activity and membrane binding ability. *Biochemistry.* **40**, 6819–6827 (2001).

[67] Joo, Youngsung., Schuman, M.C., Goldberg, J.k., Kim, S.G., Yon, F., Brütting, C., and Baldwin, I.T. Herbivore-induced volatile blends with both “fast” and “slow” components provide robust indirect defence in nature. *Funct Ecol.* **32**, 136–149 (2018).

[68] Tanaka, T., Ikeda, A., Shiojiri, K., Ozawa, R., Shiki, K., Nagai-Kunihiro, N., Fujita, K., Sugimoto, K., Yamato, K.T., Dohra, H., Ohnishi, T., Koeduka, T., and Matsui, K. Identification of a hexenal reductase that modulates the composition of green leaf volatiles, *Plant Physiol.* **178,** 552–564 (2018).

[69] Peters-Golden, M., Brock, T.G. 5-Lipoxygenase and FLAP. *Prostaglandins Leukot. Essent. Fatty Acids*. **69**, 99–109 (2003).

[70] Markoutsa, S., Sürün, D., Karas, M., Hofmann, B., Steinhilbe, D., Sorg, B.L. Analysis of 5-lipoxygenase phosphorylation on molecular level by MALDI-MS. *FEBS J.* **281**, 1931–1947 (2014).

[71] Rådmark, O., Werz, O., Steinhilber, D., Samuelsson, B. 5-Lipoxygenase: regulation of expression and enzyme activity. *Trends Biochem. Sci.* **32**, 332–341 (2007).

[72] Rådmark, O., Samuelsson, B. Regulation of the activity of 5-lipoxygenae, a key enzyme in leukotriene biosynthesis. *Biochem. Biophys. Res. Commun.* **396**, 105–110 (2010).

ACKNOWLEDGMENT

I wish to express my sincere thanks to Professor Dr. Kenji Matsui, Department of Biological Chemistry, Faculty of Agriculture, Yamaguchi University for his kind guidance, suggestions and encouragement. I am also grateful to Assistant Professor Dr. Takao Koeduka, Professor Dr. Jun'ichi Mano, and Assistant Professor Dr. Koichi Sugimoto, Department of Biological Chemistry, Faculty of Agriculture, Yamaguchi University for their helpful discussions and suggestions. I also thanks to Prof. Dr. Edward E. Farmer, Université de Lausanne, Switzerland, Prof. Dr. Harry J. Klee, University of Florida, USA, Prof. Dr. Ian T. Baldwin, Max Planck Institute, Germany, and Prof. Dr. Toshihiro Kumamaru, Kusyu University, Japan for providing Arabidopsis *lox2-1* mutant, *Solanum lycopersicum* cv. M82, *Nicotiana attenuate*, and *Oryza sativa* ssp. *japonica* cv. Nipponbare. Furthermore I wish to thank my parents and all members of the laboratory.

This works was supported by JSPS KAKENHI Grant Number 17J06032 (to S. Mochizuki).

LIST OF PUBLICATIONS

Publications of Related Literature

I. **Satoshi Mochizuki**, Kenji Matsui. Green leaf volatile-burst in *Arabidopsis* is governed by galactolipid oxygenation by a lipoxygenase that is under control of calcium ion. *Biochemical and Biophysical Research Communications.* Nov. 2018. **505**: 939–944. doi: 10.1016/j.bbrc.2018.10.042.

II. **Satoshi Mochizuki**, Koichi Sugimoto, Takao Koeduka, Kenji Matsui. Arabidopsis lipoxygenase 2 is essential for formation of green leaf volatiles and five-carbon volatiles. *FEBS Letters*. Apr. 2016. **590**: 1017–1027. doi: 10.1002/1873-3468.12133.

Publications of Reference

I. Anna Nakashima, Stephan H. von Reuss, Hiroyuki Tasaka, Misaki Nomura, **Satoshi Mochizuki**, Yoko Iijima, Koh Aoki, Daisuke Shibata, Wilhelm Boland, Junji Takabayashi, Kenji Matsui. Traumatin- and dinortraumatin-containing galactolipids in *Arabidopsis*: *their formation in tissue-disrupted leaves as counterparts of green leaf volatiles*. *The Journal of Biological Chemistry*. Sep. 2013. **288**: 26078–26088. doi: 10.1074/jbc.M113.487959.

II. Cynthia M. Mwenda, **Satoshi Mochizuki**, Kenji Matsui. Plants distinctively control green leaf volatile and jasmonate pathways, but some pathogens spike the plans. *Acta Horticulturae*. Jul. 2017. **1169**: 119–127. Doi: 10.17660/ActaHortic.2017.1169.18.

III. Kenji Matsui, **Satoshi Mochizuki**. How Do Plants Emit and Take in Volatile Organic Chemicals?: Simple Diffusion Does not Illustrate the Mechanisms. *Kagaku to Seibutsu*. Jan. 2018. **56**: 95–103.